Figure 6. Survival of leukemic precursor B-cells is suppressed when co-cultured with C/EBPβ-deficient BMMSCs. (A) BaF3/Bcr-Abl cells were co-cultured with WT or C/EBPβ-deficient (KO) BMMSCs. (B) Number of BaF3/Bcr-Abl cells when co-cultured with WT (WT, n = 5) or C/EBPβ-deficient (KO) (n = 5) BMMSCs. (C, D) Cell cycle analyses of BaF3/Bcr-Abl cells after co-culture with WT (n = 5) or C/EBPβ-deficient (KO) (n = 5) BMMSCs for 2 days. (C) Representative histograms. (D) The frequencies of BaF3/Bcr-Abl cells at G0/G1, S and G2M phases. Data are mean values ± SD. (F, G) Frequency of apoptotic BaF3/Bcr-Abl cells after co-culture with WT (n = 5) or C/EBPβ-deficient (KO) (n = 5) BMMSCs for 3days. (E) Representative counter plots. Numbers in each box indicate the percentage of cells. (F) Frequencies of Annexin V^-PI^-, Annexin V^+PI^-, and Annexin V^+PI^+ cells. Data are mean absorbance values ± SD. (G) The number of BaF3/Bcr-Abl cells stimulated with exogenous CXCL12/SDF-1 was examined by determing BrdU incorporation using a colorimetric immunoassay (n = 6). Data are mean absorbance values ± SD. *, $P < 0.05$; **, $P < 0.01$.

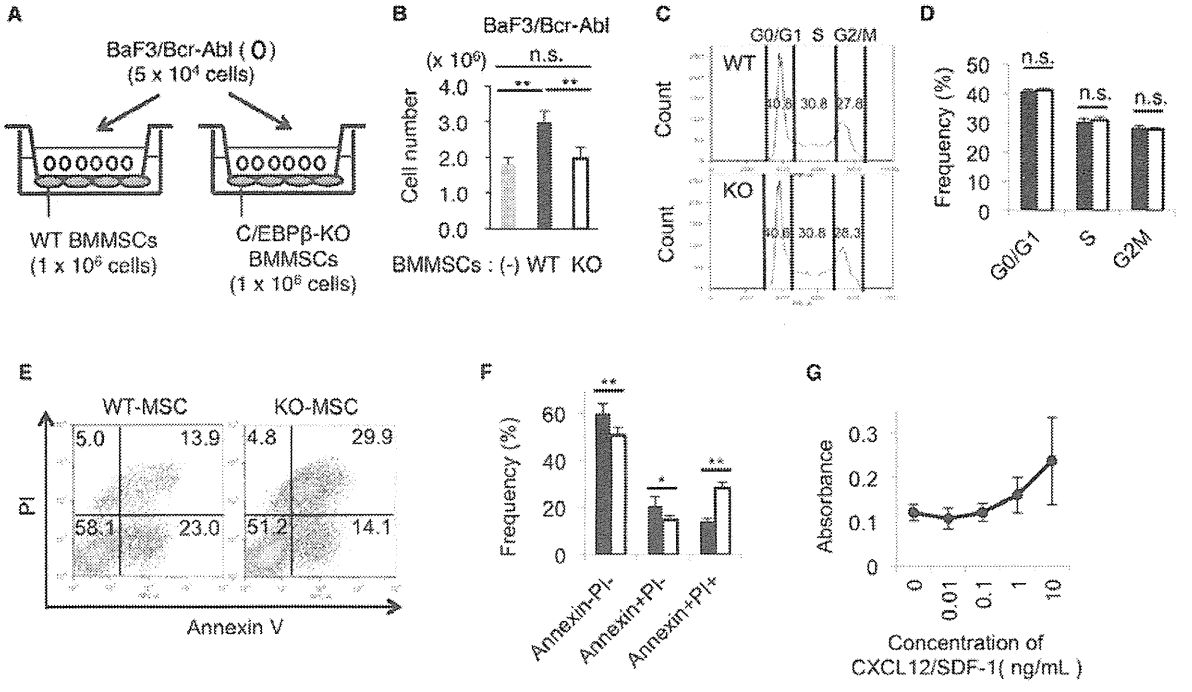

Biochemical and Biophysical Research Communications xxx (2013) xxx–xxx

Contents lists available at ScienceDirect

Biochemical and Biophysical Research Communications

journal homepage: www.elsevier.com/locate/ybbrc

Uric acid induces NADPH oxidase-independent neutrophil extracellular trap formation

Yasuyuki Arai [a,1], Yoko Nishinaka [b,c,1], Toshiyuki Arai [a,d], Makiko Morita [b], Kiyomi Mizugishi [a], Souichi Adachi [b], Akifumi Takaori-Kondo [a], Tomohiro Watanabe [e], Kouhei Yamashita [a,*]

[a] Department of Hematology and Oncology, Graduate School of Medicine, Kyoto University, Kyoto 606-8507, Japan
[b] Human Health Science, Graduate School of Medicine, Kyoto University, Kyoto 606-8507, Japan
[c] Department of Clinical Application, Center for iPS Cell Research and Application, Kyoto University, Kyoto 606-8507, Japan
[d] Department of Anesthesia, Kyoto City Hospital, Kyoto 604-8845, Japan
[e] Center for Innovation in Immunoregulative Technology and Therapeutics, Graduate School of Medicine, Kyoto University, Kyoto 606-8507, Japan

ARTICLE INFO

Article history:
Received 15 November 2013
Available online xxxx

Keywords:
Uric acid
Neutrophil extracellular trap formation
NADPH oxidase
Chronic granulomatous disease
NF-κB
Reactive oxygen species

ABSTRACT

Neutrophil extracellular traps (NETs) are composed of extracellular DNA fibers with antimicrobial peptides that capture and kill microbes. NETs play a critical role in innate host defense and in autoimmune and inflammatory diseases. While the mechanism of NET formation remains unclear, reactive oxygen species (ROS) produced via activation of NADPH oxidase (Nox) are known to be an important requirement. In this study, we investigated the effect of uric acid (UA) on NET formation. UA, a well-known ROS scavenger, was found to suppress Nox-dependent ROS release in a dose-dependent manner. Low concentrations of UA significantly inhibited Nox-dependent NET formation. However, high concentrations of UA unexpectedly induced, rather than inhibited, NET formation. NETs were directly induced by UA alone in a Nox-independent manner, as revealed by experiments using control neutrophils treated with ROS inhibitors or neutrophils of patients with chronic granulomatous disease who have a congenital defect in ROS production. Furthermore, we found that UA-induced NET formation was partially mediated by NF-κB activation. Our study is the first to demonstrate the novel function of UA in NET formation and may provide insight into the management of patients with hyperuricemia.

1. Introduction

Neutrophils, the first line of defense against the microbes, play a critical role in innate immunity [1]. In infected sites, they phagocytose microbes, degranulate enzymes, and produce reactive oxygen species (ROS) such as superoxide and hydrogen peroxide generated by the NADPH oxidase (Nox) complex. Recently, a novel killing mechanism known as neutrophil extracellular traps (NETs) has been reported. NETs capture microbes with their extracellular structures consisting of DNA fibers and antimicrobial granule proteins [2,3]. Many physiological stimuli are known to induce NETs. Notably, NET formation is generally ROS-dependent. Patients with chronic granulomatous disease (CGD), who are defective in Nox activity, fail to generate ROS and to make NETs [4]. In a recent study, we demonstrated that singlet oxygen ($^1O_2$), one species of ROS, is required for Nox-dependent NET formation on stimulation with phorbol myristate acetate (PMA) [5]. Interestingly, neutrophils of CGD patients treated with $^1O_2$ *in vitro* produced NETs, revealing that the pathway could be rescued downstream of Nox [5].

Uric acid (UA), a product of purine metabolism, is a scavenger of $^1O_2$ that regulates oxidative stress in humans [6]. Since $^1O_2$ is produced by Nox [7], UA is expected to suppress Nox-dependent NET formation. However, a recent study showed that peripheral and synovial fluid neutrophils derived from patients with acute gout, whose UA levels in serum were mostly high, formed NETs [8]. Acute gout is an inflammatory arthritis that is triggered by the deposition of monosodium urate (MSU) crystals, uric acid precipitates in sodium, into the joint space. The inflammatory cascade results in the secretion of inflammatory cytokines, especially interleukin (IL)-1ß and neutrophil recruitment into the joint [9]. Thus, it is still a matter of debate what effect UA directly exerts on NET formation.

In the present study, we first examined the effect of UA on Nox-dependent NET formation by control neutrophils stimulated with PMA. Thereafter, we investigated how UA directly affected NET for-

Abbreviations: CGD, chronic granulomatous disease; DHR, dihydrorhodamine 123; DPI, diphenyleneiodonium; HBSS, Hanks' balanced salt solution; MSU, monosodium urate; MVP, trans-1-(2′-methoxyvinyl)pyrene; Nox, NADPH oxidase; NET, neutrophil extracellular trap; PBN, α-phenyl-*N*-tert-butyl nitrone; PMA, phorbol myristate acetate; ROS, reactive oxygen species; $^1O_2$, singlet oxygen; UA, uric acid.

* Corresponding author. Fax: +81 75 751 4963.
E-mail address: kouhei@kuhp.kyoto-u.ac.jp (K. Yamashita).

[1] These authors contributed equally to this work.

0006-291X/$ - see front matter © 2013 Elsevier Inc. All rights reserved.
http://dx.doi.org/10.1016/j.bbrc.2013.12.007

mation by using control neutrophils treated with ROS inhibitors or CGD neutrophils. Finally, we demonstrate that UA may induce NET formation in a manner distinct from that of PMA.

2. Materials and methods

2.1. Reagents

Hanks' balanced salt solution (HBSS) was purchased from Invitrogen (Carlsbad, CA, USA); trans-1-(2′-methoxyvinyl)pyrene (MVP), Sytox green and orange (for double-strand DNA staining), and dihydrorhodamine 123 (DHR) were ordered from Molecular Probes (Eugene, OR, USA). α-Phenyl-*N*-tert-butyl nitrone (PBN) was acquired from Radical Research Ltd. (Hino, Tokyo, Japan) and was dissolved in phosphate-buffered saline (PBS) at a final concentration of 100 mM (pH 7.4). Anti-myeloperoxidase (MPO) antibody and matched secondary antibody (anti-rabbit IgG-Alexa Fluor 488) were obtained from Abcam (Eugene, OR, USA) and Life Technologies (Carlsbad, CA, USA), respectively. Other chemicals, including UA, PMA, diphenyleneiodonium (DPI), and apocynin, were purchased from Sigma Aldrich Inc. (St. Louis, MO, USA). (*E*)3-[(4-Methylphenyl)sulfonyl]-2-propenenitrile (BAY 11-7082) was obtained from Merck (Darmstadt, Germany).

2.2. Human CGD patients

We studied two CGD patients, a 29-year-old man with gp91-phox deficiency with a G-to-A point mutation at nucleotide 252 in exon 3, and a 24-year-old man with gp91-phox deficiency with a G-to-A point mutation at nucleotide 389 in exon 10.

2.3. Isolation of human neutrophils

Human neutrophils were isolated from peripheral blood by sedimentation through two-step Percoll (GE Healthcare, Tokyo, Japan) gradients. The experiments were conducted with the understanding and the consent of each participant. The ethical committee of Kyoto University approved the experiments.

2.4. Chemiluminescence assay

Neutrophils (2×10^6 cells) were mounted on a luminescence reader (Aloka BLR-310; Aloka, Tokyo, Japan) in the presence of 40 μM MVP, a $^1O_2$-specific probe [10]. After that, neutrophils were stimulated with 100 ng/ml PMA in the presence of 0–5 mg/dl UA, or 8 mg/dl UA alone, and MVP luminescence was monitored every 30 s for 30 min.

2.5. Flow cytometric DHR assay

Neutrophils (1×10^6 cells) treated with 2 μM DHR were stimulated with 100 ng/ml PMA or 8 mg/dl UA for 30 min at 37 °C and analyzed by flow cytometry using a FACSCanto II (Becton Dickinson, Durham, NC, USA).

2.6. Immunofluorescence stainings of NET-forming neutrophils

Purified neutrophils (1×10^5 cells) were incubated with 100 ng/ml PMA or 8 mg/dl UA in HBSS without serum for 3 h on culture slides (BD Biosciences, San Jose, CA, USA). After fixation with 2% paraformaldehyde (Nacalai Tesque, Kyoto, Japan) for 15 min and

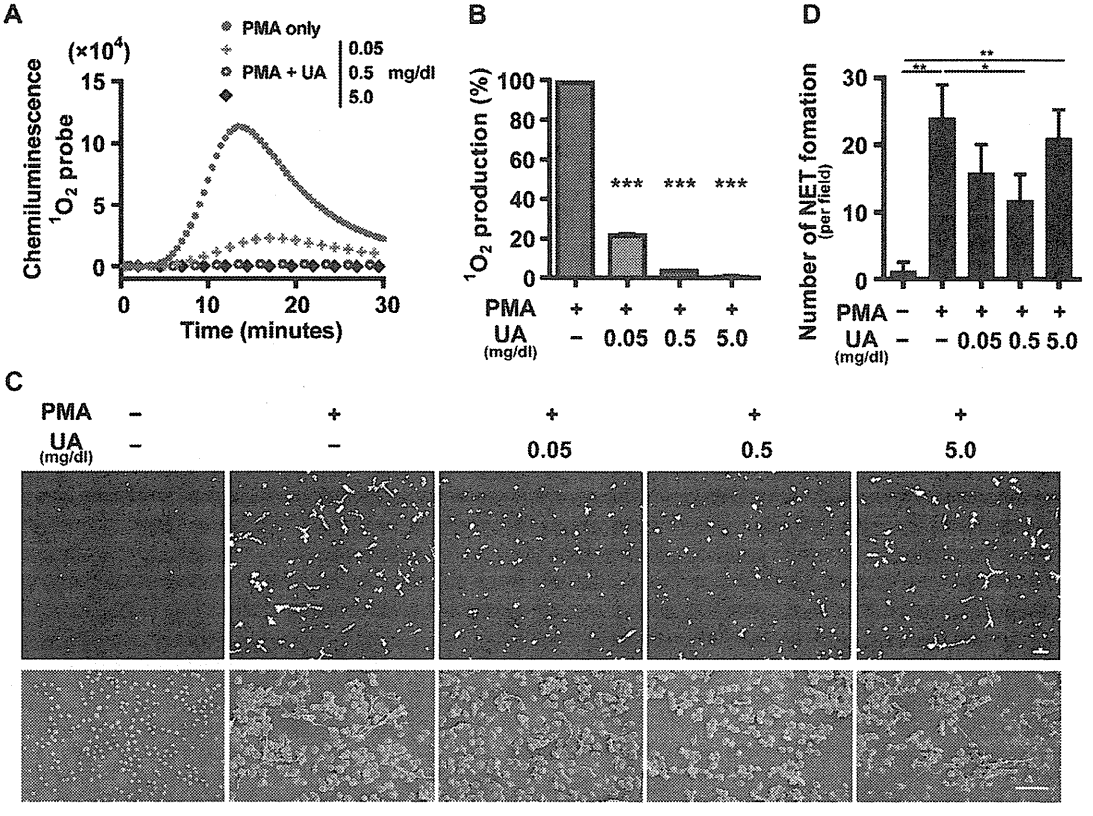

Fig. 1. The effect of UA on PMA-induced ROS production and NET formation. Neutrophils were isolated from the peripheral blood of healthy volunteers. (A) The effect of UA (0–5 mg/dl) on $^1O_2$ production by PMA-stimulated neutrophils. The $^1O_2$ production by neutrophils was examined by chemiluminescence using a $^1O_2$-specific probe, MVP. (B) Quantitative analysis of $^1O_2$ production by neutrophils. The $^1O_2$ production is shown relative to that by PMA-stimulated neutrophils in the absence of UA. The data represent the mean ± SE ($n = 3$, $^{***}P < 0.001$, unpaired *t*-test). (C) The effect of UA on PMA-induced NET formation. Neutrophils stimulated with PMA were incubated with 0–5 mg/dl UA. NET formation was visualized by laser-scanning fluorescence confocal microscopy (upper panels) and SEM (lower panels). Scale bars represent 100 μm (upper panels) and 30 μm (lower panels). (D) Quantitative analysis of NET formation. The data represent the mean ± SE ($n = 4$, $^{*}P < 0.05$, $^{**}P < 0.01$, unpaired *t*-test).

Please cite this article in press as: Y. Arai et al., Uric acid induces NADPH oxidase-independent neutrophil extracellular trap formation, Biochem. Biophys. Res. Commun. (2013), http://dx.doi.org/10.1016/j.bbrc.2013.12.007

permeabilization with 100% methanol (Nacalai Tesque) for 10 min at -20 °C, the cells were stained with rabbit anti-MPO antibodies overnight at 4 °C, followed by Alexa Fluor 488-conjugated goat anti-rabbit IgG and Sytox orange. The cells were attached to the slides by centrifugation, coverslipped with mounting medium (ProLong Gold Antifade Reagent, Life Technologies), and analyzed by confocal microscopy.

2.7. NET formation by neutrophils

Neutrophils (4×10^6 cells) from healthy volunteers were suspended in HBSS without serum and stimulated with 100 ng/ml PMA in the presence of 0–5 mg/dl UA for 3 h at 37 °C under 5% CO_2 in glass base dish (Asahi Glass, Tokyo, Japan). In other experiments, neutrophils from healthy volunteers or CGD patients were stimulated with 1–8 mg/dl UA alone. After incubation, cells were stained with 500 nM Sytox Green, and NET formation was visualized with a laser-scanning fluorescence confocal microscope (Nikon Digital Eclipse C1, Tokyo, Japan). Quantitative analysis was performed by counting the number of NET-forming cells per field (average data of 5 randomly selected fields). NET formation was also visualized with a scanning electron microscope (SEM, S-4700, Hitachi, Tokyo, Japan).

2.8. Treatments of neutrophils with inhibitors

Neutrophils (4×10^6 cells) from healthy volunteers were pre-incubated at 37 °C for 30 min with Nox inhibitors, DPI (10 μM) and apocynin (10 μM), a $^1O_2$ inhibitor, PBN (4 mM) [11], or an NF-κB inhibitor, Bay 11-7082 (10 μM), and then stimulated with 100 ng/ml PMA or 8 mg/dl UA for 3 h. NET formation was visualized and analyzed as described above.

2.9. Immunoblotting

Neutrophils (4×10^6 cells) from healthy volunteers were incubated at 37 °C for 30 min with 100 ng/ml PMA or 8 mg/dl UA. Lysates were prepared using RIPA lysis buffer (Wako Pure Chemical Industries, Osaka, Japan). Cell debris was separated by centrifugation and equal amounts of proteins in the supernatant were separated by electrophoresis (4–12% SDS–polyacrylamide gels, Life Technologies). Proteins were then electrotransferred onto nitrocel-

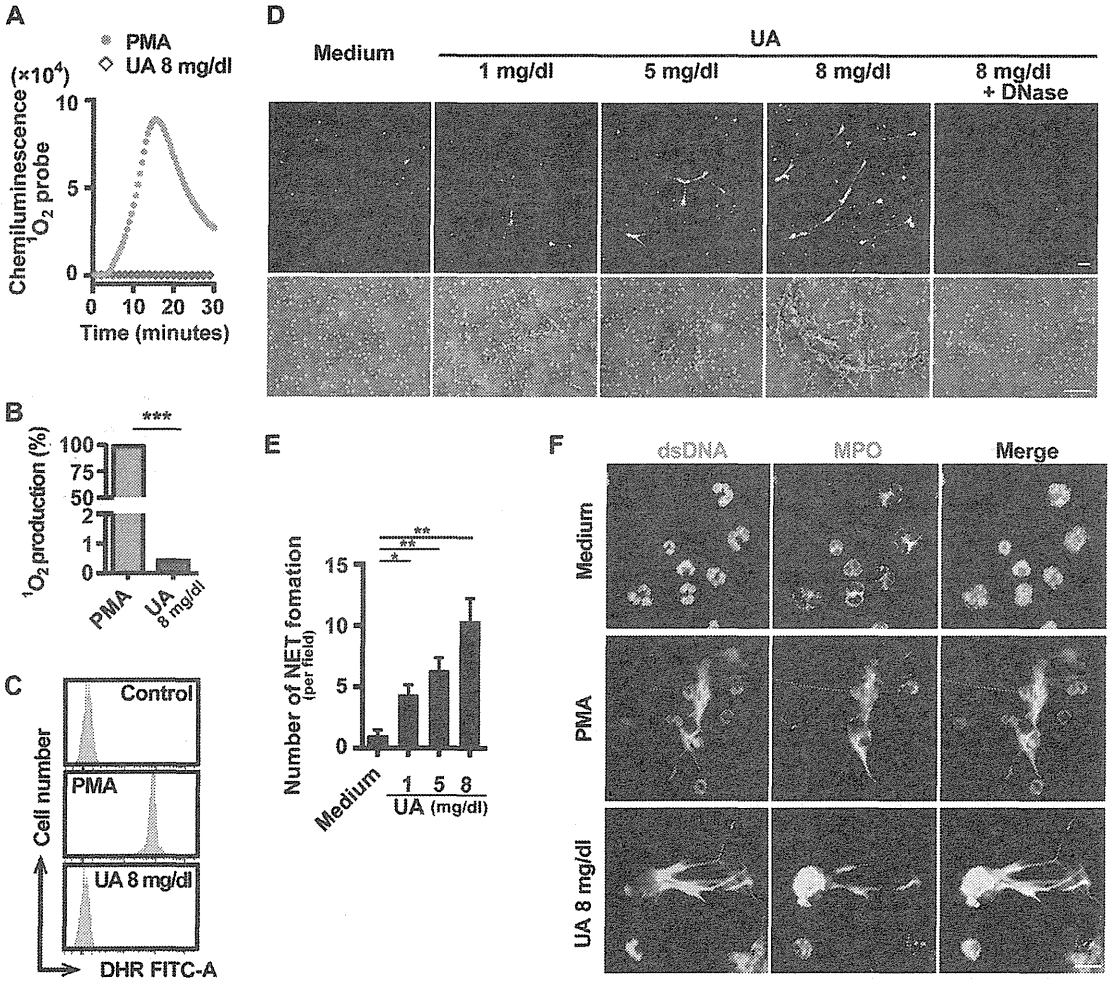

Fig. 2. The effect of UA alone on ROS production and NET formation. (A and B) Effect of UA on $^1O_2$ production. Neutrophils were stimulated with PMA (100 ng/ml) or UA (8 mg/dl). $^1O_2$ production was examined by chemiluminescence using a $^1O_2$-specific probe, MVP. (A) Representative data. UA-stimulated neutrophils hardly produced any $^1O_2$. (B) Quantitative analysis of $^1O_2$ production shown relative to that by PMA-stimulated neutrophils. Data represent mean ± SE ($n = 3$, $^{***}P < 0.001$, unpaired t-test). (C) ROS production by DHR assay. The logarithmic fluorescence intensity is shown on the x-axis and the cell count on the y-axis. (D–F) Direct effect of UA on NET formation. (D) Representative micrographs of neutrophils incubated with 1–8 mg/dl of UA. NET formation was visualized by laser-scanning fluorescence confocal microscopy (upper panels) and SEM (lower panels). Scale bars represent 100 μm (upper panels) and 30 μm (lower panels). (E) Quantitative analysis of NET formation. Data represent the mean ± SE ($n = 5$, $^{*}P < 0.05$, $^{**}P < 0.01$, unpaired t-test). (F) Colocalization of extracellular dsDNA and MPO in UA-stimulated neutrophils. UA- or PMA-stimulated neutrophils were immunostained with anti-MPO antibody (green). The dsDNAs were counterstained with Sytox-orange (red). Scale bars represent 10 μm. (For interpretation of the references to color in this figure legend, the reader is referred to the web version of this article.)

Please cite this article in press as: Y. Arai et al., Uric acid induces NADPH oxidase-independent neutrophil extracellular trap formation, Biochem. Biophys. Res. Commun. (2013), http://dx.doi.org/10.1016/j.bbrc.2013.12.007

lulose membranes. After blocking, membranes were incubated overnight at 4 °C with a rabbit polyclonal anti-phospho-NF-κB p65 or anti-NF-κB p65 antibody (Santa Cruz Biotechnology, Dallas, TX, USA) followed by a goat anti-rabbit HRP antibody. Protein bands were visualized by enhanced chemiluminescence, and results were analyzed with ImageJ software.

2.10. Statistical analysis

Data were expressed as mean ± standard error (SE). Values of $P < 0.05$ determined by the unpaired Student t-test were considered significant.

3. Results and discussion

We examined the effect of UA on $^1O_2$ production and NET formation by PMA-stimulated neutrophils. First, neutrophils from healthy volunteers were stimulated with PMA with or without UA, and the $^1O_2$ production was detected by chemiluminescence. As expected, increasing concentrations of UA (0.05–5 mg/dl) suppressed $^1O_2$ production by PMA-stimulated neutrophils in a dose-dependent manner, suggesting that UA is a $^1O_2$ scavenger (Fig. 1A and B). Treatments of less than 0.5 mg/dl of UA suppressed PMA-induced NET formation in confocal microscopy (Fig. 1C, upper panels, and Fig. 1D) and SEM (Fig. 1C, lower panels). Surprisingly, treatment of PMA-stimulated neutrophils with 5 mg/dl of UA failed to suppress NET formation, suggesting that a high concentration of UA may have a novel function in NET formation (Fig. 1C and D). These results were substantiated by the quantitative analysis of representative micrographs (Fig. 1D).

Next, we investigated the direct effect of UA on $^1O_2$ production and NET formation. UA treatment alone did not produce any detectable levels of $^1O_2$ (Fig. 2A and B). We used the fluorescent dye DHR in a flow cytometric assay to detect ROS. UA-stimulated neutrophils from healthy volunteers did not exhibit any increase in DHR fluorescence, in contrast to a significant increase in PMA-stimulated neutrophils (Fig. 2C). Unexpectedly, UA alone

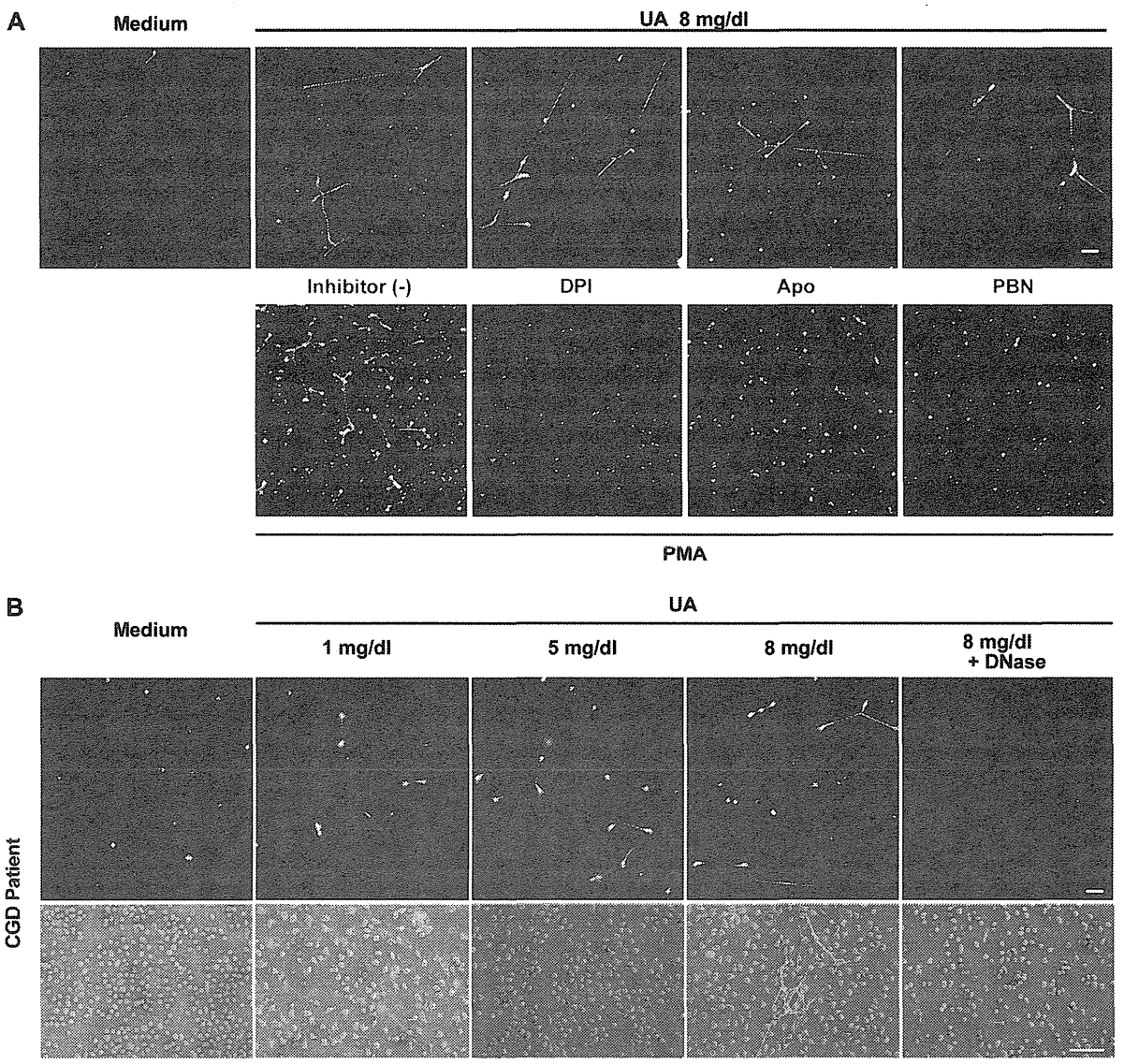

Fig. 3. UA-induced NET formation is independent of ROS. (A) The effect of ROS inhibitors on UA- (upper panels) or PMA- (lower panels) induced NET formation. Neutrophils from healthy volunteers were incubated with 8 mg/dl UA or 100 ng/ml PMA in the presence or absence of Nox inhibitors, DPI and apocynin (Apo), or a $^1O_2$ inhibitor, PBN. NET formation was visualized by laser-scanning fluorescence confocal microscopy. Scale bars represent 100 μm. (B) The effect of UA on NET formation. Neutrophils from CGD patients were incubated with 1–8 mg/dl of UA. Representative micrographs are shown. NET formation was visualized by laser-scanning fluorescence confocal microscopy (upper panels) and SEM (lower panels). Scale bars represent 100 μm (upper panels) and 30 μm (lower panels).

Please cite this article in press as: Y. Arai et al., Uric acid induces NADPH oxidase-independent neutrophil extracellular trap formation, Biochem. Biophys. Res. Commun. (2013), http://dx.doi.org/10.1016/j.bbrc.2013.12.007

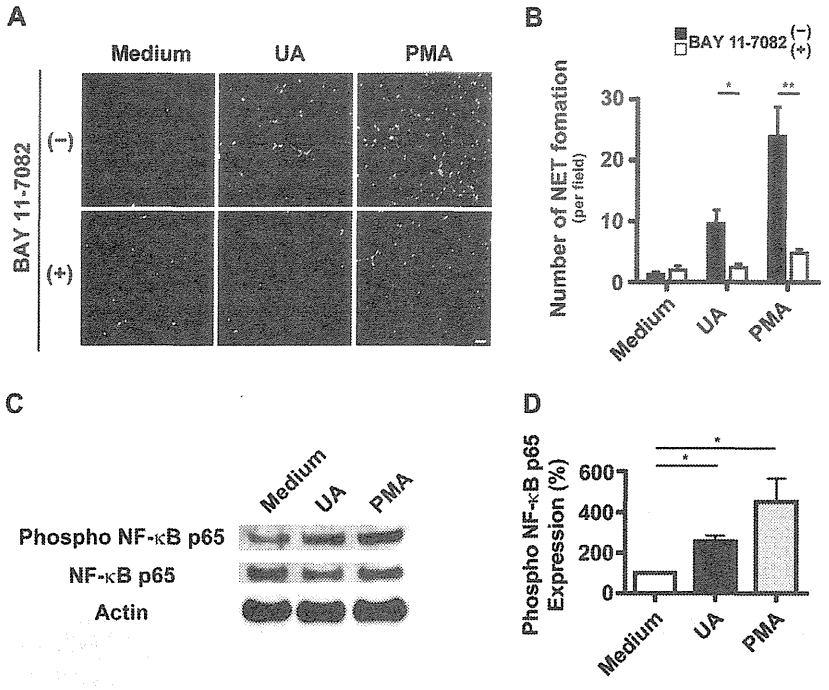

Fig. 4. UA induces NET formation through NF-κB activation. (A and B) The effect of an NF-κB inhibitor on UA-induced NET formation. Neutrophils from healthy volunteers were stimulated with 100 ng/ml PMA or 8 mg/dl UA in the presence or absence of an NF-κB inhibitor. (A) Representative micrographs. NET formation was visualized by laser-scanning fluorescence confocal microscopy. Scale bars represent 100 μm. (B) Quantitative analysis of NET formation. The data represent the mean ± SE ($n = 5$, $^*P < 0.05$, $^{**}P < 0.01$, unpaired *t*-test). (C) Immunoblot analysis of PMA- or UA-stimulated neutrophils. Cell lysates were subjected to immunoblotting using an anti-phospho-NF-κB p65 or anti-NF-κB p65 antibody. Membranes were reprobed with an anti-actin antibody. (D) Quantification of proteins on immunoblots. The expression levels are shown relative to that in neutrophils without stimuli. The data represent the mean ± SE ($n = 5$, $^*P < 0.05$, unpaired *t*-test).

significantly induced NET formation in healthy neutrophils, irrespective of the absence of ROS (Fig. 2D and E). NET formation was abrogated by DNase treatment, which degrades DNA fibers of NETs (Fig. 2D). NET formation by UA was further verified by immunostaining, in which extracellular dsDNA colocalized with a granule protein MPO, an important structural component of NETs (Fig. 2F). These results suggest that NET formation by UA may not be mediated by ROS.

This hypothesis was substantiated by the use of Nox inhibitors, DPI and apocynin, or a $^1O_2$ scavenger, PBN. None of the ROS inhibitors suppressed UA-induced NET formation, while PMA-induced NETs were strongly inhibited (Fig. 3A). We next examined NET formation in neutrophils from CGD patients, who have a defect in ROS formation. Regardless of the absence of ROS, CGD neutrophils treated with UA produced NETs, which were suppressed by DNase treatment (Fig. 3B). Taken together, these results suggest that UA may induce NET formation in a Nox-independent manner.

Recently, Lopponi et al. implicated NF-κB activation in NET formation induced by PMA stimulus or stress signals, such as acidic or hyperthermic conditions [12]. Therefore, we investigated whether NF-κB blockade affected NET formation by UA-stimulated neutrophils. The treatment of healthy neutrophils with the NF-κB inhibitor BAY 11-7082 resulted in a marked suppression of UA-induced NET formation (Fig. 4A and B). In addition, immunoblot analysis revealed that phosphorylation of the p65 subunit of NF-κB was significantly enhanced in neutrophils stimulated with UA (Fig. 4C and D). Taken together, these results suggest that the NF-κB cascade is important in UA-mediated NET formation, and could be a key regulatory pathway of NET formation. Identification of signaling pathways upstream of NF-κB in UA-induced NET formation should be a future area of investigation.

In summary, this is the first report to demonstrate the novel function of UA in NET formation. Contrary to expectations, UA, a known $^1O_2$ scavenger, induced NETs in neutrophils in a Nox-independent manner and partially through activation of the NF-κB pathway. The mechanisms by which UA contributes to NET formation are not yet clear. It has been reported that the Raf-MEK-ERK pathway is involved in a NET formation cascade downstream of Nox activation in PMA-stimulated neutrophils [13]. Furthermore, MSU crystals induced NETs in a ROS-dependent manner as well as PMA [14]. In contrast, NET formation by UA was independent of ROS. In addition, neither the activation of ERK, nor the suppression of NETs by an ERK inhibitor, was observed in UA-stimulated neutrophils in our study (unpublished observation). This suggests that UA induces NETs in a different fashion from that of PMA and MSU crystals. An example of ROS-independent NET formation was reported in a recent study, where the calcium ionophore ionomycin did not require Nox activation to induce NETs [15]. Moreover, *Staphylococcus aureus* and *Candida albicans* have been reported to induce NETs independently of Nox [16,17]. Thus, it is possible that there are several mechanisms of NET formation. The importance of a ROS-independent pathway in NET formation in physiological settings awaits further investigation.

NETs are similar to a double-edged sword; they can either fight disease or cause disease, depending on the situation [18]. Excessive NET formation is associated with the pathogenesis of inflammatory and autoimmune diseases, including preeclampsia [19], cystic fibrosis [20], and systemic lupus erythematosus [21]. Moreover, NETs are relevant to vascular injury, in which extracellular histones released from neutrophils during NET formation injure the endothelium [22], and the injured endothelium, in turn, induces NETs, establishing a vicious cycle leading to severe damage [23]. Clinically, the association of hyperuricemia and gout with other medical conditions such as hypertension, chronic kidney disease, and cardiovascular disease has been recognized [24]. Recent animal and epidemiologic studies support the idea that uric acid elevation in the serum is an independent risk factor for the development of these serious medical problems, by damaging

Please cite this article in press as: Y. Arai et al., Uric acid induces NADPH oxidase-independent neutrophil extracellular trap formation, Biochem. Biophys. Res. Commun. (2013), http://dx.doi.org/10.1016/j.bbrc.2013.12.007

endothelial cells, although it is still a matter of debate [25]. In light of these findings, we speculate that uric acid elevation may induce NET formation and subsequent vascular endothelial dysfunction, ultimately leading to cardiovascular diseases. Therefore, NETs could be a missing link between uric acid elevation and cardiovascular diseases. Thus, we may need to reappraise the importance of uric acid in human health and disease, and reconsider the management of patients with asymptomatic hyperuricemia in order to decrease the risk of cardiovascular diseases.

Conflict of interest disclosure

The authors declare no conflict of interest.

Acknowledgments

We thank Keiko Furuta and Haruyasu Kohda (Division of Electron Microscopic Study, Center for Anatomical Studies, Graduate School of Medicine, Kyoto University) for excellent technical assistance. This research was supported by Grants-in-aid for scientific research from the Japan Society for the Promotion of Science (23591474) to K.Y.

References

[1] C. Nathan, Neutrophils and immunity: challenges and opportunities, Nat. Rev. Immunol. 6 (2006) 173–182.
[2] V. Brinkmann, U. Reichard, C. Goosmann, B. Fauler, Y. Uhlemann, D.S. Weiss, Y. Weinrauch, A. Zychlinsky, Neutrophil extracellular traps kill bacteria, Science 303 (2004) 1532–1535.
[3] V. Brinkmann, A. Zychlinsky, Beneficial suicide: why neutrophils die to make NETs, Nat. Rev. Microbiol. 5 (2007) 577–582.
[4] T.A. Fuchs, U. Abed, C. Goosmann, R. Hurwitz, I. Schulze, V. Wahn, Y. Weinrauch, V. Brinkmann, A. Zychlinsky, Novel cell death program leads to neutrophil extracellular traps, J. Cell Biol. 176 (2007) 231–241.
[5] Y. Nishinaka, T. Arai, S. Adachi, A. Takaori-Kondo, K. Yamashita, Singlet oxygen is essential for neutrophil extracellular trap formation, Biochem. Biophys. Res. Commun. 413 (2011) 75–79.
[6] B.N. Ames, R. Cathcart, E. Schwiers, P. Hochstein, Uric acid provides an antioxidant defense in humans against oxidant- and radical-caused aging and cancer: a hypothesis, Proc. Natl. Acad. Sci. U.S.A. 78 (1981) 6858–6862.
[7] S.J. Klebanoff, Myeloperoxidase: friend and foe, J. Leukocyte Biol. 77 (2005) 598–625.
[8] I. Mitroulis, K. Kambas, A. Chrysanthopoulou, P. Skendros, E. Apostolidou, I. Kourtzelis, G.I. Drosos, D.T. Boumpas, K. Ritis, Neutrophil extracellular trap formation is associated with IL-1beta and autophagy-related signaling in gout, PLoS One 6 (2011) e29318.
[9] E.B. Gonzalez, An update on the pathology and clinical management of gouty arthritis, Clin. Rheumatol. 31 (2012) 13–21.
[10] G.H. Posner, J.R. Lever, K. Miura, C. Lisek, H.H. Seliger, A. Thompson, A chemiluminescent probe specific for singlet oxygen, Biochem. Biophys. Res. Commun. 123 (1984) 869–873.
[11] A. Kawai, Y. Nishinaka, T. Arai, K. Hirota, H. Mori, N. Endo, T. Miyoshi, K. Yamashita, M. Sasada, Alpha-phenyl-*N*-tert-butyl nitrone has scavenging activity against singlet oxygen ((1)O(2)) and attenuates (1)O(2)-induced neuronal cell death, J. Pharmacol. Sci. 108 (2008) 545–549.
[12] M.J. Lapponi, A. Carestia, V.I. Landoni, L. Rivadeneyra, J. Etulain, S. Negrotto, R.G. Pozner, M. Schattner, Regulation of neutrophil extracellular trap formation by anti-inflammatory drugs, J. Pharmacol. Exp. Ther. 345 (2013) 430–437.
[13] A. Hakkim, T.A. Fuchs, N.E. Martinez, S. Hess, H. Prinz, A. Zychlinsky, H. Waldmann, Activation of the Raf-MEK-ERK pathway is required for neutrophil extracellular trap formation, Nat. Chem. Biol. 7 (2011) 75–77.
[14] C. Schorn, C. Janko, V. Krenn, Y. Zhao, L.E. Munoz, G. Schett, M. Herrmann, Bonding the foe – NETting neutrophils immobilize the pro-inflammatory monosodium urate crystals, Front. Immunol. 3 (2012) 376.
[15] H. Parker, M. Dragunow, M.B. Hampton, A.J. Kettle, C.C. Winterbourn, Requirements for NADPH oxidase and myeloperoxidase in neutrophil extracellular trap formation differ depending on the stimulus, J. Leukocyte Biol. 92 (2012) 841–849.
[16] F.H. Pilsczek, D. Salina, K.K. Poon, C. Fahey, B.G. Yipp, C.D. Sibley, S.M. Robbins, F.H. Green, M.G. Surette, M. Sugai, M.G. Bowden, M. Hussain, K. Zhang, P. Kubes, A novel mechanism of rapid nuclear neutrophil extracellular trap formation in response to Staphylococcus aureus, J. Immunol. 185 (2010) 7413–7425.
[17] A.S. Byrd, X.M. O'Brien, C.M. Johnson, L.M. Lavigne, J.S. Reichner, An extracellular matrix-based mechanism of rapid neutrophil extracellular trap formation in response to Candida albicans, J. Immunol. 190 (2013) 4136–4148.
[18] V. Brinkmann, A. Zychlinsky, Neutrophil extracellular traps: is immunity the second function of chromatin?, J. Cell Biol. 198 (2012) 773–783.
[19] A.K. Gupta, P. Hasler, W. Holzgreve, S. Gebhardt, S. Hahn, Induction of neutrophil extracellular DNA lattices by placental microparticles and IL-8 and their presence in preeclampsia, Hum. Immunol. 66 (2005) 1146–1154.
[20] R. Manzenreiter, F. Kienberger, V. Marcos, K. Schilcher, W.D. Krautgartner, A. Obermayer, M. Huml, W. Stoiber, A. Hector, M. Griese, M. Hannig, M. Studnicka, L. Vitkov, D. Hartl, Ultrastructural characterization of cystic fibrosis sputum using atomic force and scanning electron microscopy, J. Cyst. Fibros. 11 (2012) 84–92.
[21] A. Hakkim, B.G. Furnrohr, K. Amann, B. Laube, U.A. Abed, V. Brinkmann, M. Herrmann, R.E. Voll, A. Zychlinsky, Impairment of neutrophil extracellular trap degradation is associated with lupus nephritis, Proc. Natl. Acad. Sci. U.S.A. 107 (2010) 9813–9818.
[22] J. Xu, X. Zhang, R. Pelayo, M. Monestier, C.T. Ammollo, F. Semeraro, F.B. Taylor, N.L. Esmon, F. Lupu, C.T. Esmon, Extracellular histones are major mediators of death in sepsis, Nat. Med. 15 (2009) 1318–1321.
[23] A.K. Gupta, M.B. Joshi, M. Philippova, P. Erne, P. Hasler, S. Hahn, T.J. Resink, Activated endothelial cells induce neutrophil extracellular traps and are susceptible to NETosis-mediated cell death, FEBS Lett. 584 (2010) 3193–3197.
[24] D.I. Feig, D.H. Kang, R.J. Johnson, Uric acid and cardiovascular risk, N. Engl. J. Med. 359 (2008) 1811–1821.
[25] N.L. Edwards, The role of hyperuricemia in vascular disorders, Curr. Opin. Rheumatol. 21 (2009) 132–137.

Please cite this article in press as: Y. Arai et al., Uric acid induces NADPH oxidase-independent neutrophil extracellular trap formation, Biochem. Biophys. Res. Commun. (2013), http://dx.doi.org/10.1016/j.bbrc.2013.12.007

European Journal of Haematology

ORIGINAL ARTICLE

Antitumor effects of bevacizumab in a microenvironment-dependent human adult T-cell leukemia/lymphoma mouse model

Fumiko Mori[1], Takashi Ishida[1], Asahi Ito[1], Fumihiko Sato[2], Ayako Masaki[1], Tomoko Narita[1], Susumu Suzuki[2], Tomiko Yamada[1], Hisashi Takino[2], Masaki Ri[1], Shigeru Kusumoto[1], Hirokazu Komatsu[1], Masakatsu Hishizawa[3], Kazunori Imada[4], Akifumi Takaori-Kondo[3], Akio Niimi[1], Ryuzo Ueda[5], Hiroshi Inagaki[2], Shinsuke Iida[1]

[1]Department of Medical Oncology and Immunology, Nagoya City University Graduate School of Medical Sciences, Nagoya;[2]Department of Anatomic Pathology and Molecular Diagnostics, Nagoya City University Graduate School of Medical Sciences, Nagoya; [3]Department of Hematology and Oncology, Graduate School of Medicine, Kyoto University, Kyoto; [4]Department of Hematology, Kokura Memorial Hospital, Kitakyushu; [5]Department of Tumor Immunology, Aichi Medical University School of Medicine, Nagakute, Japan

Abstract

Objective: The objective of this study was to evaluate the therapeutic potential of bevacizumab with or without systemic chemotherapy for adult T-cell leukemia/lymphoma (ATL) and clarify the significance of angiogenesis for ATL pathogenesis. *Methods:* NOD/Shi-*scid*, IL-2Rγ^{null} (NOG) mice were used as recipients of tumor cells from a patient with ATL, which engraft and proliferate in a microenvironment-dependent manner. The ATL cells could be serially transplanted in NOG mice, but could not be maintained in *in vitro* cultures. *Results:* Injection of bevacizumab alone significantly increased necrosis and decreased vascularization in the tumor tissue. Levels of human soluble interleukin two receptor in the serum (reflecting the ATL tumor burden) of bevacizumab-treated mice were significantly lower than in untreated mice. Although bevacizumab monotherapy showed these clear anti-angiogenesis effects, it did not prolong survival. In contrast, injection of bevacizumab together with cyclophosphamide, doxorubicin, vincristine, prednisolone (CHOP) led to a significant prolongation of survival of the ATL mice relative to CHOP alone. *Conclusions:* This is the first report to evaluate the efficacy of bevacizumab for ATL in a tumor microenvironment-dependent model. Bevacizumab therapy combined with chemotherapy could be a valuable treatment strategy for that subgroup of ATL probably depending to a large extent on angiogenesis via vascular endothelial growth factor.

Key words Adult T-cell leukemia-lymphoma; Bevacizumab; tumor microenvironment

Correspondence Takashi Ishida, MD, PhD, Department of Medical Oncology and Immunology, Nagoya City University Graduate School of Medical Sciences, 1 Kawasumi, Mizuho-chou, Mizuho-ku, Nagoya, Aichi 467-8601, Japan. Tel: +81 52 853 8216; Fax: +81 52 852 0849; e-mail: itakashi@med.nagoya-cu.ac.jp

Accepted for publication 29 October 2013

doi:10.1111/ejh.12231

Adult T-cell leukemia-lymphoma (ATL) is an aggressive peripheral T-cell neoplasm caused by human T-cell lymphotropic virus type 1 (HTLV-1). The disease is resistant to conventional chemotherapeutic agents, and currently there are only limited treatment options; thus, it has a very poor prognosis (1–4). Over the past decade, allogeneic hematopoietic stem-cell transplantation has evolved into a potential approach to treating patients with ATL. However, only a small fraction of patients have the opportunity to benefit from transplantation, such as those who are younger, have achieved sufficient disease control, and have an appropriate stem-cell source (5, 6). Therefore, the development of alternative treatment strategies for patients with ATL is an urgent issue.

Bevacizumab is a humanized monoclonal antibody against the vascular endothelial growth factor A (VEGF-A), a key

factor inducing the formation of blood vessels (angiogenesis) in tumors (7). Bevacizumab is currently approved worldwide for the treatment of several types of cancer such as metastatic colorectal cancer, metastatic non-small-cell lung cancer, renal cell carcinoma, and advanced ovarian cancer, in combination with chemotherapy or interferon (8–14). Bevacizumab is also approved as a single agent for recurrent glioblastoma in the USA (15). In this context, many aspects of pathological angiogenesis have been extensively studied in many types of cancer. On the other hand, the precise role of these processes in pathogenesis of hematological malignancies including ATL is still under active investigation (16–19). Thus far, bevacizumab has not been approved for the treatment of any hematological malignancy in the USA, Europe, or Japan. The aim of the present study was to evaluate the therapeutic potential of bevacizumab with or without systemic chemotherapy for ATL and clarify the significance of angiogenesis for ATL pathogenesis, using a microenvironment-dependent murine ATL model.

Methods

Animals

NOD/Shi-*scid*, IL-2Rγ^{null} (NOG) mice (20) were purchased from the Central Institute for Experimental Animals (Kanagawa, Japan) and used at 6–8 wk of age. All of the *in vivo* experiments were performed in accordance with the United Kingdom Coordinating Committee on Cancer Research Guidelines for the Welfare of Animals in Experimental Neoplasia, Second Edition, and were approved by the Ethics Committee of the Center for Experimental Animal Science, Nagoya City University Graduate School of Medical Sciences.

Immunopathological analysis

We assessed the affected lymph nodes of 23 patients with ATL by immunopathology. The patients provided written informed consent in accordance with the Declaration of Helsinki, and this present study was approved by the institutional Ethics Committee of Nagoya City University Graduate School of Medical Sciences. Hematoxylin and eosin (HE) staining and immunostaining using anti-human CD4 (4B12; Novocastra, Wetzlar, Germany), CD25 (4C9; Novocastra), CD20 (L26; DAKO, Glostrup, Denmark), VEGF-A (sc-152, rabbit polyclonal; Santa Cruz, Heidelberg, Germany), Alpha-Smooth Muscle Actin (α-SMA) (1A4; DAKO), CD31 (JC70A; DAKO), and von Willebrand Factor (Rabbit polyclonal; DAKO) were performed on formalin-fixed, paraffin-embedded sections. VEGF-A expression levels were categorized according to the following formula: 3+ positive if ≥50%, 2+ positive if <50 ≥30%, 1+ positive if <30 ≥10%, and negative if <10% of the ATL tumor cells were stained with the corresponding antibody. Nine 100× high-power fields (HPF) of HE tumor specimens were randomly selected, and the area of tumor necrosis (%) was calculated by Image J software (21), and then averaged. Nine 100× HPF of von Willebrand Factor-stained tumor specimens were randomly selected, and numbers of vessels (per mm^2) were calculated by Image J software and then averaged.

ATL mouse model

A leukemic cell clone from a patient with ATL, which could be serially transplanted into SCID mice, designated S-YU as reported previously (22), was injected intraperitoneally (i.p.) into NOG mice. Three to 4 wk after i.p. injection, NOG mice were presented with intraperitoneal masses along the mesentery. Cells from these intraperitoneal masses were suspended in RPMI-1640 and inoculated i.p. into healthy NOG mice, which then presented with features identical to those of the original mice.

Cell lines

ATN-1, MT-1, and TL-Om1 are ATL cell lines, whereas MT-2, MT-4, and TL-Su are HTLV-1-immortalized lines, as previously described (23).

Quantitative reverse transcription-polymerase chain reaction

Total RNA was isolated with RNeasy Mini Kits (QIAGEN, Tokyo, Japan). Reverse transcription from the RNA to first strand cDNA was carried out using High Capacity RNA-to-cDNA Kits (Applied Biosystems Inc, Foster City, CA, USA). *Human VEGF-A* (Hs00900055_m1), *VEGF-R1* (Hs00176573_m1), *VEGF-R2* (Hs00911700_m1), and *β-actin* (Hs99999903_m1) *mRNA* were amplified using TaqMan® Gene Expression Assays with the aid of an Applied Biosystems StepOnePlus™. The quantitative assessment of the mRNA of interest was done by dividing its level by that of *β-actin* and expressing the result relative to Human Testis Total RNA (Clontech, Mountain View, CA, USA) as 1.0. All expressed values were averages of triplicate experiments.

Monoclonal antibodies and flow cytometry

The following Monoclonal antibodies (mAbs) were used for flow cytometry: APC-conjugated anti-human CD45 mAb (2D1; BD Biosciences, San Jose, CA, USA), PerCP-conjugated anti-CD4 mAb (SK3; BD Biosciences), PE-conjugated anti-CD25 mAb (M-A251; BD Biosciences), PE-conjugated VEGF-R1 mAb (49560; BD Biosciences), PE-conjugated VEGF-R2 mAb (89106, R&D Systems, Inc. Minneapolis, MN,

USA), and the appropriate isotype control mAbs. Whole blood was treated with BD FACS lysing solution (BD Biosciences) to remove RBC. Stained cells were analyzed on a FACSCalibur (BD Biosciences) with the aid of FlowJo software (Tree Star, Inc. Ashland, OR, USA).

Cell proliferation assay

Proliferation of S-YU and HTLV-I-immortalized lines expressing both VEGF-A and VEGF-R1 in the presence of different concentrations of bevacizumab for 48 h was assessed using CellTiter 96 Aqueous One Solution cell proliferation assay kits (Promega Corporation, Madison, WI, USA). Bevacizumab was purchased from Chugai Pharmaceutical Co., Ltd., Tokyo, Japan.

ATL cell-bearing mice treated with bevacizumab

ATL tumor cells (S-YU) from the intraperitoneal masses were suspended in RPMI-1640, and 1.0×10^7 was inoculated i.p. into each of 14 NOG mice. The animals were divided into two groups of seven each for treatment with bevacizumab or to serve as controls. Bevacizumab (10 mg/kg) or vehicle (saline) was i.p. injected into the mice 3, 10, and 17 d after tumor cell inoculations. Therapeutic efficacies were evaluated for area of tumor necrosis, number of vessels, and serum human sIL2R levels 22 d after tumor inoculation. The concentration of human sIL2R in the serum was measured by ELISA using human sIL2R immunoassay kits (R&D Systems, Inc.).

ATL cells from the intraperitoneal masses suspended in RPMI-1640 were also inoculated i.p. into another 10 NOG mice at 1.0×10^7 per mouse. These animals were randomly divided into two groups of five each for treatment with bevacizumab or as controls. Bevacizumab (10 mg/kg) or saline was injected i.p. into the mice 2, 9, 16, and 23 d after tumor cell inoculation. Therapeutic efficacy of bevacizumab was evaluated by survival times.

A further 16 NOG mice that had also received 1.0×10^7 ATL cells from intraperitoneal masses were randomly divided into two groups of eight each for treatment with bevacizumab + cyclophosphamide, doxorubicin, vincristine, prednisolone (CHOP) or CHOP alone. Bevacizumab (10 mg/kg) or saline was i.p. injected into the mice 2, 9, 16, 23, 30, and 37 d after tumor cell inoculations. CHOP was given i.p. 17 d after tumor inoculation at the following doses: cyclophosphamide, 40 mg/kg; doxorubicin, 3.3 mg/kg; vincristine, 0.5 mg/kg; and prednisolone, 0.2 mg/kg (24, 25). Therapeutic efficacy of bevacizumab was evaluated by survival time. Cyclophosphamide and vincristine were purchased from Shionogi Pharmaceutical Co., Ltd, Osaka, Japan; doxorubicin was from Kyowa Hakko Kirin Co., Ltd, Tokyo, Japan, and prednisolone was from Nippon Kayaku Co., Ltd, Tokyo, Japan.

Statistical analysis

The differences between groups regarding the tumor necrosis area, vascular number, and human sIL2R concentrations in serum were analyzed by the Mann–Whitney *U* test. In this study, $P < 0.05$ was considered significant.

Results

VEGF-A expression in ATL

VEGF-A expression by ATL cells in the lymph node lesions is shown in Fig. 1A. Immunopathological features of four cases from each group stratified by VEGF-A expression are shown in Fig. 1B. Most of the ATL cases (96%) were positive for VEGF-A.

ATL cell-bearing NOG mice

In earlier studies, S-YU ATL tumor cells, which were serially transplanted into SCID mice (22), manifested multiple enlarged mesenteric lymph nodes. In the present study, in which NOG mice rather than SCID mice were the S-YU recipients, larger tumor masses formed along the intestinal tract. Figure 2A shows the intraperitoneal masses and intestinal tract adhering tightly to one another in a NOG mouse (demarcated by thin white dotted lines in the figure). Flow cytometric analysis demonstrated that the mass mainly consisted of human cells expressing CD4 and CD25 (Fig. 2B). Immunopathological analysis revealed large atypical cells with irregular and pleomorphic nuclei, and blood vessels. The cells were CD4-positive, CD25-positive, but CD20-negative (Fig. 2C). These findings are consistent with an ATL cell phenotype in humans, and with earlier studies in the SCID/S-YU model. The S-YU tumor cells in the NOG mice were classed as VEGF-A 1+ positive (Fig. 2C). Blood vessels in the tumor tissue were stained by anti-α-SMA Ab (Fig. 2C). Vascular endothelial cells in the tumor tissue were stained by anti-von Willebrand Factor Ab, but not by anti-CD31 mAb (data not shown). Together, these results show that the blood vessels in the tumor tissue originated from the mouse, because anti-α-SMA and von Willebrand Factor Ab used in this study recognized the corresponding protein derived from both human and mouse, whereas the anti-CD31 mAb recognized the corresponding human but not murine protein (data not shown). CD4-positive CD25-positive ATL cell mild infiltration into spleen, liver, and bone marrow was seen by flow cytometry (Fig. 2D).

VEGF-A, VEGF-R1, and -R2 expression in ATL and HTLV-1-immortalized lines

VEGF-A mRNA expression was detected in all 7 ATL and HTLV-1-immortalized lines tested, and in S-YU cells

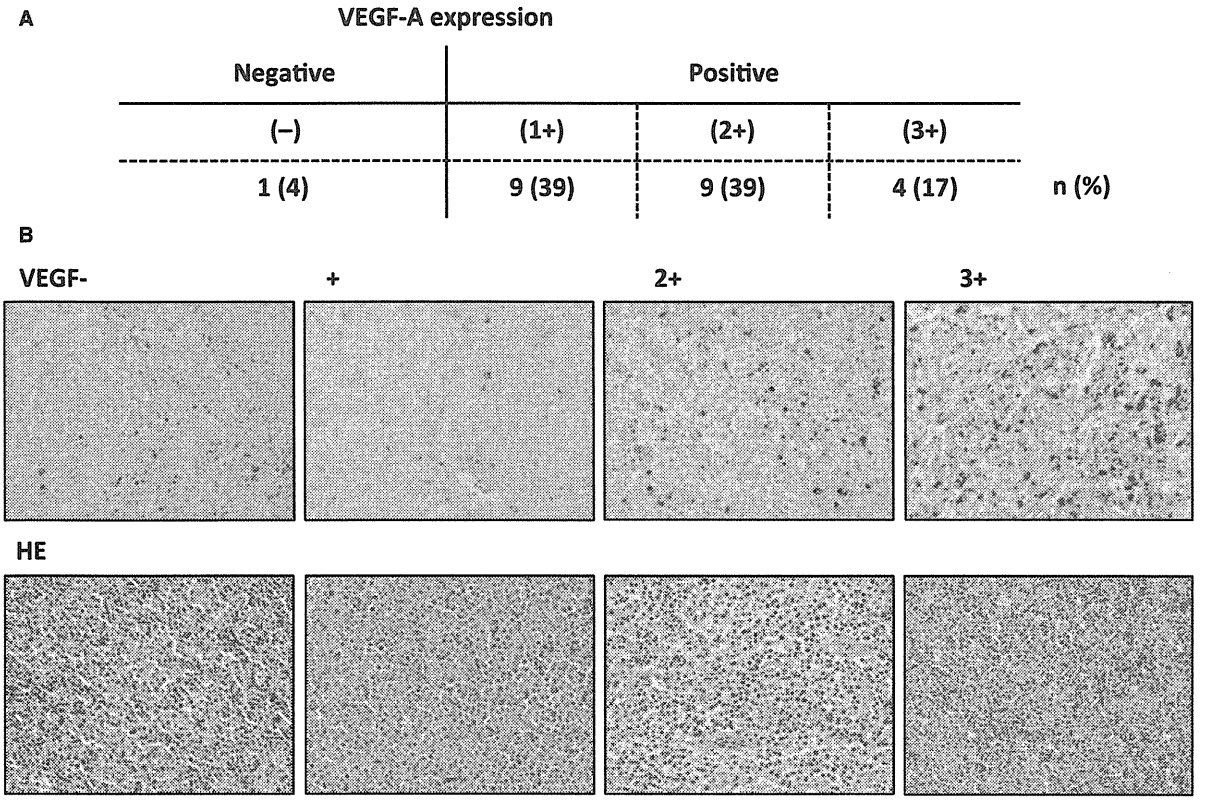

Figure 1 Vascular endothelial growth factor A (VEGF-A) expression in ATL. (A) VEGF-A expression of ATL cells in the lymph node lesion. VEGF-A expression was categorized based on the percentage of ATL cells stained as follows: ≥50%, 3+ positive; 30–49%, 2+ positive; 10–29%, 1+ positive; <10%, negative. (B) Cases 1, 2, 3, and 4 are representative of VEGF-A-negative, 1+, 2+, and 3+ positive categories, respectively. Photomicrographs with VEGF-A (upper panels) and hematoxylin and eosin staining (lower panels) are shown.

from intraperitoneal masses (Fig. 3A, upper left panel). *VEGF-R1 mRNA* expression was not present in ATL and in only two HTLV-1-immortalized lines (MT-2 and TL-Su) but was present in S-YU cells (Fig. 3A, upper right panel). No *VEGF-R2 mRNA* expression was detected in any of the 7 ATL and HTLV-1-immortalized lines tested, or in S-YU cells (data not shown). Flow cytometry demonstrated that VEGF-R1 protein was also expressed in MT-2 and TL-Su, and very weakly in NOG S-YU cells (Fig. 3A, lower panels), consistent with the RT-PCR results. Flow cytometry demonstrated that VEGF-R2 was not expressed at all in any of the ATL and HTLV-1-immortalized lines tested, or in S-YU cells (data not shown), which was also consistent with the RT-PCR results.

VEGF-R1 and VEGF-R2 expression in primary ATL cells

CD4-positive CD25-positive primary ATL cells in PBMC obtained from nine individual patients with ATL (i–ix) were evaluated for VEGF-R1 and -R2 expression. VEGF-R1 protein was expressed in only one patient (patient v) and VEGF-R2 was not expressed in any of the patients (Fig. 4B).

No Bevacizumab-mediated anti-proliferative activity against HTLV-1-immortalized lines and S-YU *in vitro*

Bevacizumab did not directly block the proliferation of MT-2 and TL-Su cells *in vitro*, despite their expression of both VEGF-A and VEGF-R1. Neither did it inhibit S-YU cells (Fig. 3C).

Therapeutic efficacy of bevacizumab monotherapy in S-YU cell-bearing NOG mice

Photomicrographs of tumor tissue from each mouse are shown (Fig. 4A). Treatment with bevacizumab resulted in an increased percentage of tumor necrosis in the NOG/S-YU mice (mean 25.3%, median 24.1%, range 19.2–33.6%), compared to control mice (mean 15.9%, median 15.4%, range 11.7–21.0%, $P = 0.0060$) (Fig. 4B, left panel). An example of calculating the percentage necrotic area is presented in Fig. 4B, right-hand panels. Bevacizumab treatment resulted in decreased vascular number in the tumor tissues [3.1, 2.6,

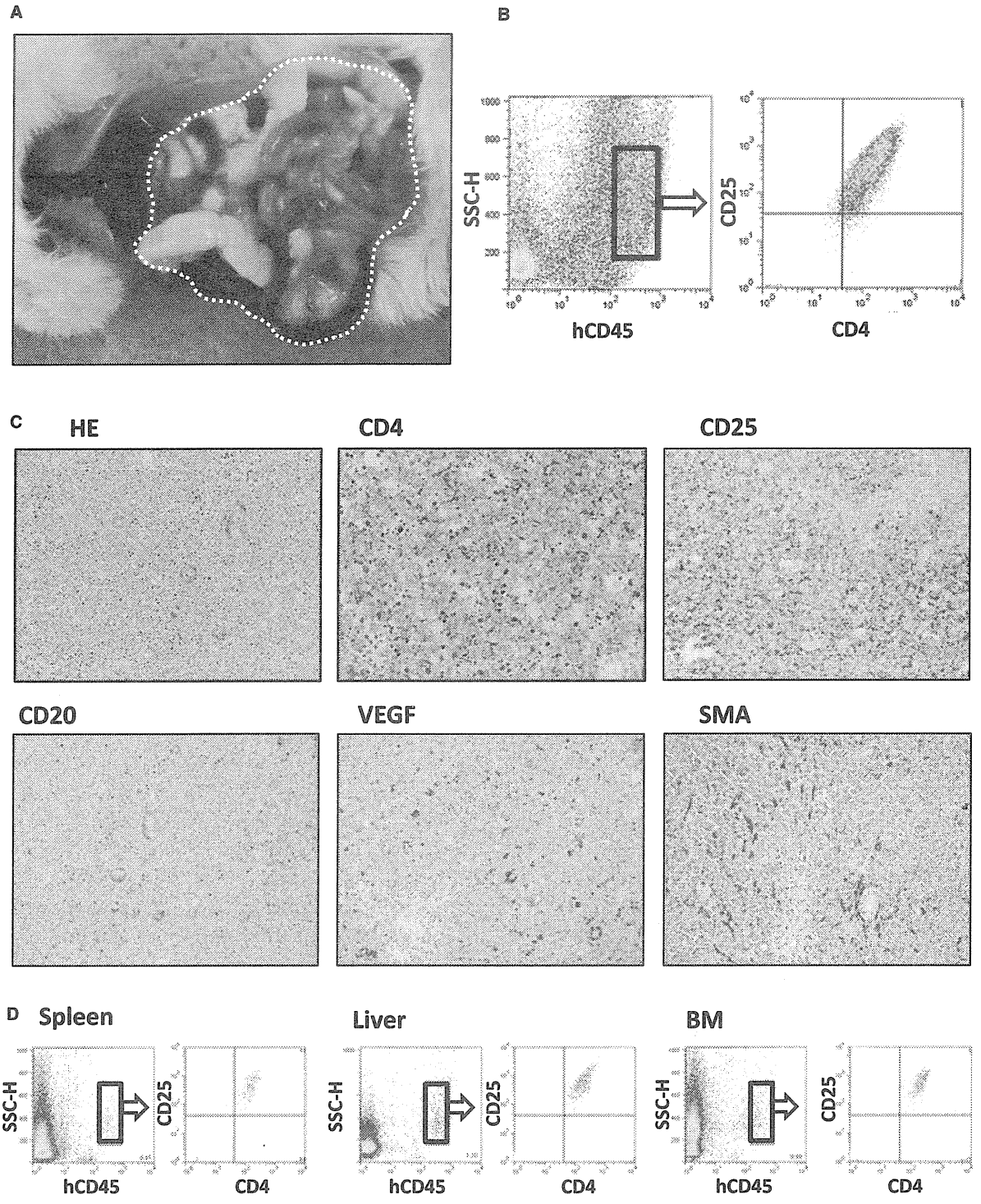

Figure 2 ATL cell-bearing NOG mouse model. (A) Macroscopic appearance of a primary DLBCL cell-bearing ATL mouse. The intraperitoneal mass is demarcated by a thin white dotted line. (B) Human CD45-positive cells in the mass determined by human CD4 and CD25 expression. (C) Immunohistochemical images of the intraperitoneal mass. (D) Human CD45-positive cells of each organ determined by human CD4 and CD25 expression.

0.0–8.3/mm^2; (mean, median, range)], compared to controls (12.8, 15.6, 1.6–19.3/mm^2, P = 0.0127) (Fig. 4C, left panel). An example of this calculation is presented in Fig. 4C, right-hand panels. Because sIL2R appears in the serum, concomitant with its increased expression on cells, we measured human sIL2R concentrations as a surrogate marker reflecting

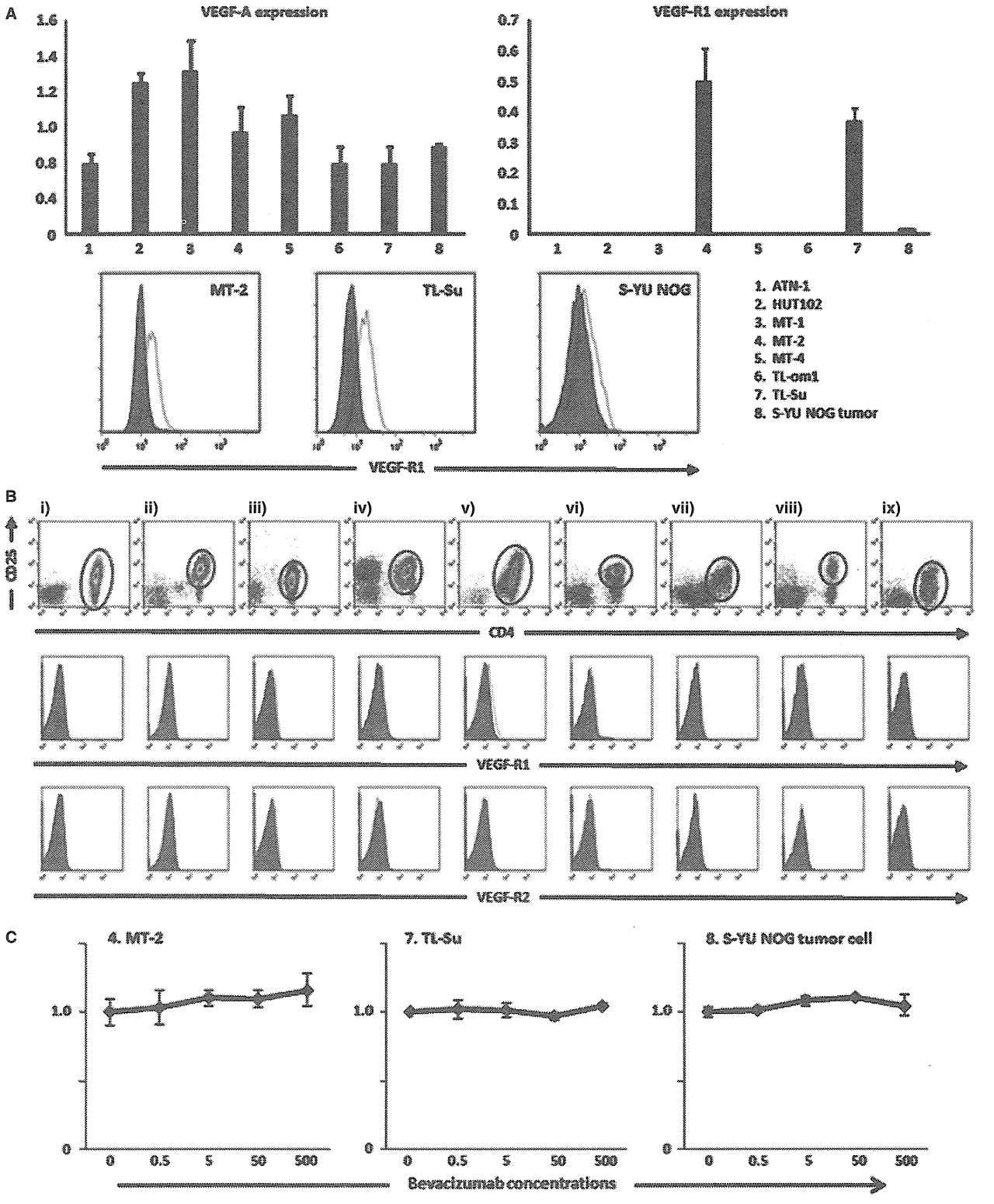

Figure 3 Vascular endothelial growth factor A (VEGF-A), VEGF-R1, and -R2 expression in primary ATL cells, or ATL and HTLV-1-immortalized lines (A) Quantitative RT-PCR analysis for VEGF-A and VEGF-R1 in 7 ATL and HTLV-1-immortalized lines, and NOG ATL cells from the intraperitoneal mass (upper panels). Flow cytometry for VEGF-R1 in HTLV-1-immortalized lines MT-2 and TL-Su, and NOG ATL cells, from the intraperitoneal mass (lower panels). (B) Flow cytometry for VEGF-R1, and -R2 in 9 primary ATL cells. (C) Bevacizumab has no direct anti-proliferative activity against HTLV-1-immortalized lines (MT-2 and TL-Su) expressing both VEGF-A and VEGF-R1, or NOG ATL cells, *in vitro*. Each result represents three independent experiments.

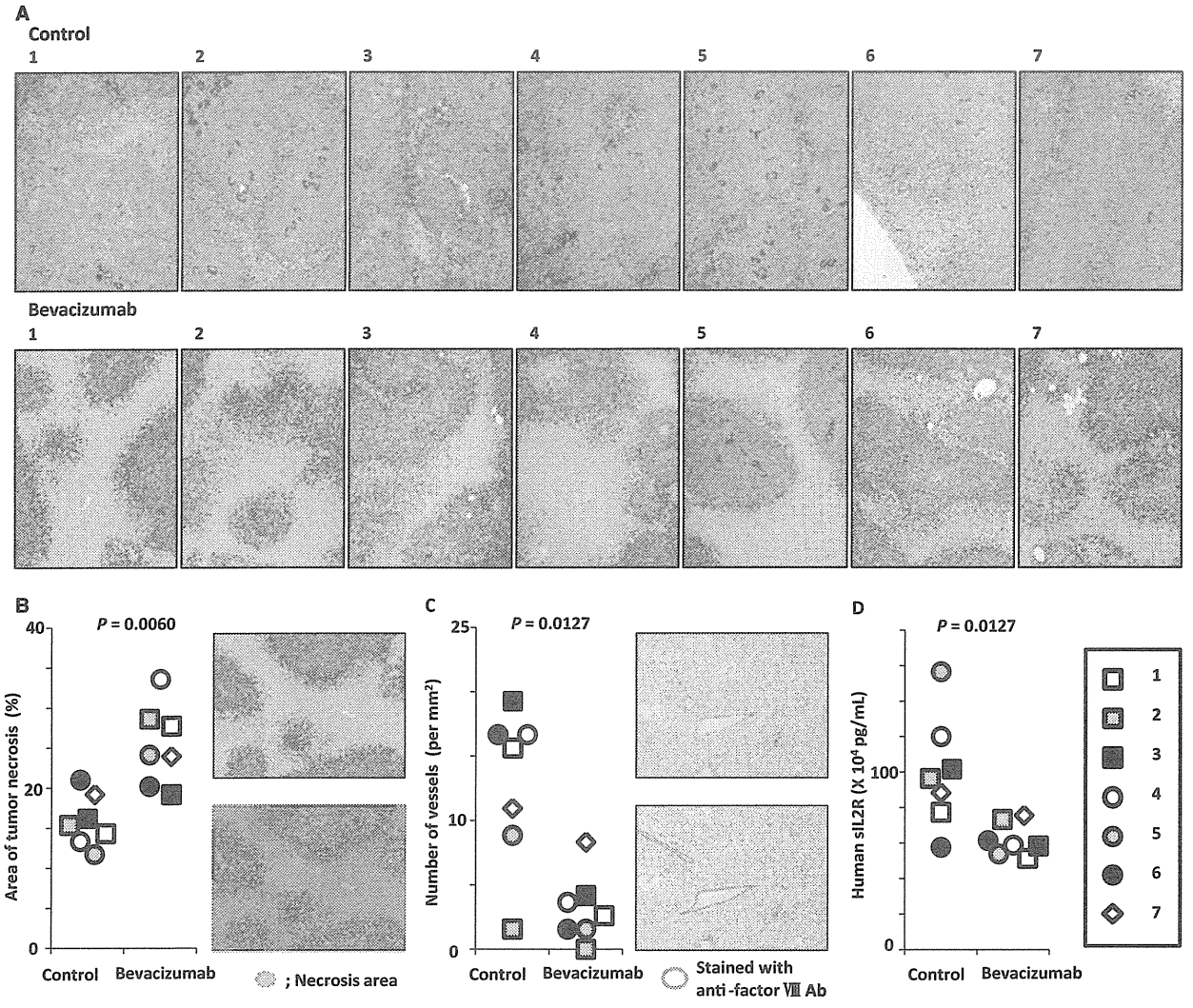

Figure 4 Bevacizumab therapy has significant therapeutic efficacy in the ATL cell-bearing NOG mouse model. (A) Macroscopic photomicrographs with hematoxylin and eosin staining of mice given saline (control) (upper panels) or bevacizumab (lower panels). (B) Area of tumor necrosis (%) of each ATL cell-bearing NOG mouse. The bevacizumab-treated mice had significantly greater tumor necrosis than control mice (left panel). An example of a calculation for tumor necrosis area (%) by means of Image J software is shown (right panels). (C) Numbers of vessels (/mm^2) of each ATL cell-bearing NOG mouse. The bevacizumab recipients had significantly fewer vessels than controls (left panel). An example of such a calculation by means of Image J software is shown (right panels). (D) Serum sIL2R concentrations of each ATL cell-bearing NOG mouse. The bevacizumab recipients had significantly lower levels of sIL2R than controls.

the tumor burden of the human CD25-expressing ATL (26). Treatment with bevacizumab showed significantly greater therapeutic efficacy as demonstrated by sIL2R concentrations in S-YU cell-bearing NOG mice (617.9, 588.5, 513.2–755.7 $\times$ 10^3 pg/mL), compared to controls (996.6, 963.4, 575.7–1565.0 $\times$ 10^3 pg/mL, P = 0.0127) (Fig. 4D). Although bevacizumab monotherapy showed significant therapeutic efficacy as demonstrated by the percentage of tumor necrosis, vascular number in the tumor tissues, and sIL2R concentrations in sera (Fig. 4), it did not confer any survival advantage to the NOG/S-YU mice (Fig. 5A). No toxicity attributable to bevacizumab injections was observed in any of the mice in this setting.

Therapeutic efficacy of bevacizumab plus CHOP compared to CHOP alone in S-YU cell-bearing NOG mice

The bevacizumab plus CHOP group did have a significant prolongation of survival compared with CHOP alone (P = 0.046). The median survival time of bevacizumab plus CHOP and CHOP alone was 38 and 34 d, respectively.

Discussion

In this study, we have demonstrated that bevacizumab possesses significant therapeutic efficacy in an ATL mouse model in which the tumor cells from a patient survive and

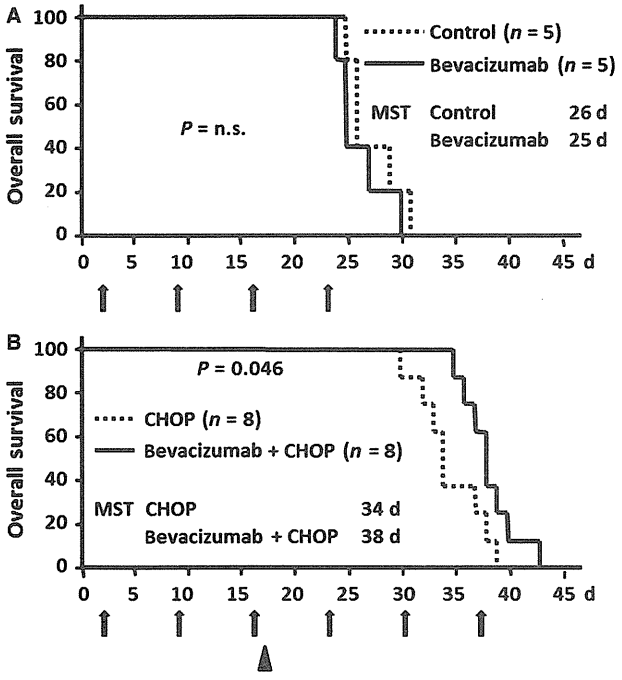

Figure 5 Survival analysis of ATL cell-bearing NOG mice treated with bevacizumab (A) Kaplan–Meier survival curves of ATL cell-bearing NOG mice treated with bevacizumab or saline. Arrows, bevacizumab or control (saline) injections. Each group consists of five mice. The difference between the bevacizumab and control groups is not significant. (B) Kaplan–Meier survival curves of ATL cell-bearing NOG mice treated with bevacizumab + CHOP, or CHOP alone. Arrows, bevacizumab or control (saline) injections. Arrow head, CHOP injection. Each group consists of eight mice. The difference between the bevacizumab + CHOP and CHOP alone is statistically significant.

proliferate in a murine microenvironment-dependent manner. The present finding revealed the importance of angiogenesis for the pathogenesis of VEGF-expressing ATL.

NOG mice have severe, multiple immune defects, such that human immune cells engrafted into them retain essentially the same functions as in humans (27, 28). While it has been reported that S-YU cells can be serially transplanted into SCID mice as recipients, the present study demonstrated that S-YU cells could also be serially transplanted into NOG mice. This was not unexpected given the even more severe immune dysfunction of NOG mice compared to SCID mice. This may also explain why the ATL tumor masses were much larger in NOG than in SCID mice.

In this study, most primary ATL cases (22/23), and all of the established cell lines tested (7/7), were positive for VEGF-A. These results are consistent with data from other investigators (16, 18, 19). Thus, the VEGF-A produced by ATL cells is likely to play an important role in the pathogenesis of ATL. On the other hand, *VEGF-R1 mRNA* expression was only seen in two of the seven ATL and HTLV-1-immortalized lines, and *VEGF–R2* in none of them. VEGF-R1 protein expression by primary ATL tumor cells was only seen in one of nine patients, and VEGF-R2 in none. In B-cell lymphomas, an earlier study reported that tumor cell growth was promoted in an autocrine fashion via VEGF-A/VEGF-R1 or VEGF-A/VEGF-R2 interactions (29). However, the present analysis of VEGF-R1/R2 expression in ATL, and the results of *in vitro* proliferation assays, did not support the existence of such an autocrine loop in ATL.

Because S-YU cells can only be maintained by serial transplantation in immunodeficient mice, but not by *in vitro* culture (30), the microenvironment is likely to be indispensable for their survival. S-YU are positive for VEGF-A, and therefore it would be expected that the interaction of VEGF-A produced by ATL cells with receptors on host (murine) endothelial cells should play an important role in tumor angiogenesis. This would lead to tumor cell survival and proliferation supported by transport of sufficient nutrients and oxygen in the mouse. Therefore, the present ATL model using S-YU should better reflect the human ATL *in vivo* environment, compared to other mouse models using established ATL cell lines, or HTLV-1-immortalized lines. Thus, this model should provide a powerful tool for understanding the pathogenesis of ATL. Furthermore, it should be useful not only for evaluating novel cytotoxic anti-ATL agents, but also provide a more appropriate *in vivo* model to test antitumor agents targeting the microenvironment, including bevacizumab.

The effect observed in mice receiving bevacizumab monotherapy, as demonstrated by the increased tumor necrosis area and reduced vasculature in the tumor tissue, was expected, given the conventional antitumor mechanism of bevacizumab, which neutralizes the human VEGF-A produced by the tumor cells, but not murine VEGF-A (31). It then inhibits the growth of new blood vessels and thus starves tumor cells of necessary nutrients and oxygen (32). This should lead to a reduced tumor burden, as indicated by the sIL2R concentrations measured. Although bevacizumab monotherapy did show this anti-angiogenesis effect, it did not lead to survival prolongation in this study. This finding is consistent with the clinical observations in many types of cancer such as colorectal cancer, non-small-cell lung cancer, renal cell carcinoma, and ovarian cancer. On the other hand, combination treatment with bevacizumab and CHOP did prolong survival compared to CHOP alone. Nonetheless, the extent of this prolongation was not marked, which is also consistent with clinical observations in many types of cancer where bevacizumab is of limited benefit and then only when combined with chemotherapy. This study suggested that the tumor cell 'starvation effect' alone mediated by bevacizumab does not result in prolonged survival. It has been reported that VEGF-targeted therapy can 'normalize' the tumor vascular network and that this can lead to a more uniform blood flow, with subsequent increased delivery of chemotherapeutic agents (33, 34). This normalization by bevacizumab is a possible explanation for the prolonged survival in the present combination setting.

The present study demonstrated the importance of angiogenesis for the pathogenesis of ATL and the potential efficacy of blocking this in at least a subgroup of patients with ATL. In recent clinical cancer therapy experience, the epidermal growth factor receptor (EGFR) tyrosine kinase inhibitor, gefitinib, failed to yield significantly improved overall survival in patients with refractory NSCLC, but did show therapeutic benefit in a subgroup of patients with mutated EGFR (35). In the case of mAb targeting the EGFR, both panitumumab and cetuximab also yield clinical benefits only in a subgroup of colorectal cancer patients with wild-type *KRAS* and BRAF (36). These findings indicate that we should develop novel treatment strategies based on tumor biology, and not on tumor category. Therefore, as a next step, further investigations are warranted to determine which subgroups of patients with ATL will benefit from bevacizumab therapy (37). In other words, we should face the challenge of developing robust biomarkers that can guide selection of those patients with ATL for whom bevacizumab therapy will be most beneficial. In addition, several promising new agents for treating ATL are currently being developed (1, 38–40). Investigations of combinations of bevacizumab with these novel agents are also warranted.

In conclusion, to the best of our knowledge this is the first report to evaluate the efficacy of bevacizumab for ATL in a tumor microenvironment-dependent animal model. Bevacizumab therapy combined with chemotherapy could be a potential treatment strategy for that subgroup of patients with ATL probably depending to a large extent on angiogenesis via VEGF for tumor survival and proliferation.

Acknowledgements

We thank Ms Chiori Fukuyama for her excellent technical assistance and Ms. Naomi Ochiai for her excellent secretarial assistance.

Funding

This study was supported by Grants-in-Aid for Scientific Research (B) (No. 25290058, T. Ishida), and Scientific Support Programs for Cancer Research (No. 221S0001, T. Ishida) from the Ministry of Education, Culture, Sports, Science and Technology of Japan, Grants-in-Aid for National Cancer Center Research and Development Fund (No. 21-6-3, T. Ishida), and H23-Third Term Comprehensive Control Research for Cancer-general-011, T. Ishida, from the Ministry of Health, Labour and Welfare, Japan.

Authorship contributions

Mori F, Ishida T, Asahi I, and Ueda R designed the research. Mori F, Ishida T, Asahi I, Sato F, Masaki A, Narita T, Suzuki S, Yamada T, and Takino H performed the research. Hishizawa M, Imada K, Takaori-Kondo A contributed to establishing the ATL mouse model. All the authors analyzed the data and wrote the article.

Conflict of interest

Nagoya City University Graduate School of Medical Sciences has received research funding for Takashi Ishida, Shigeru Kusumoto, and Shinsuke Iida from Chugai Pharmaceutical Co., Ltd. The other authors have no financial conflicts of interest related with this study.

References

1. Ishida T, Ueda R. Antibody therapy for adult T-cell leukemia-lymphoma. *Int J Hematol* 2011;**94**:443–52.
2. Matsuoka M, Jeang KT. Human T-cell leukaemia virus type 1 (HTLV-1) infectivity and cellular transformation. *Nat Rev Cancer* 2007;**7**:270–80.
3. Shimoyama M. Diagnostic criteria and classification of clinical subtypes of adult T-cell leukaemia-lymphoma. A report from the Lymphoma Study Group (1984–87). *Br J Haematol* 1991;**79**:428–37.
4. Uchiyama T, Yodoi J, Sagawa K, Takatsuki K, Uchino H. Adult T-cell leukemia: clinical and hematologic features of 16 cases. *Blood* 1977;**50**:481–92.
5. Ishida T, Hishizawa M, Kato K, *et al.* Allogeneic hematopoietic stem cell transplantation for adult T-cell leukemia-lymphoma with special emphasis on preconditioning regimen: a nationwide retrospective study. *Blood* 2012;**120**:1734–41.
6. Utsunomiya A, Miyazaki Y, Takatsuka Y, *et al.* Improved outcome of adult T cell leukemia/lymphoma with allogeneic hematopoietic stem cell transplantation. *Bone Marrow Transplant* 2001;**27**:15–20.
7. Carmeliet P, Jain RK. Molecular mechanisms and clinical applications of angiogenesis. *Nature* 2011;**473**:298–307.
8. Burger RA, Brady MF, Bookman MA, *et al.* Incorporation of bevacizumab in the primary treatment of ovarian cancer. *N Engl J Med* 2011;**365**:2473–83.
9. Escudier B, Pluzanska A, Koralewski P, *et al.* Bevacizumab plus interferon alfa-2a for treatment of metastatic renal cell carcinoma: a randomised, double-blind phase III trial. *Lancet* 2007;**370**:2103–11.
10. Escudier B, Bellmunt J, Négrier S, Bajetta E, Melichar B, Bracarda S, Ravaud A, Golding S, Jethwa S, Sneller V. Phase III trial of bevacizumab plus interferon alfa-2a in patients with metastatic renal cell carcinoma (AVOREN): final analysis of overall survival. *J Clin Oncol* 2010;**28**:2144–50.
11. Hurwitz H, Fehrenbacher L, Novotny W, *et al.* Bevacizumab plus irinotecan, fluorouracil, and leucovorin for metastatic colorectal cancer. *N Engl J Med* 2004;**350**:2335–42.
12. Perren TJ, Swart AM, Pfisterer J, *et al.* A phase 3 trial of bevacizumab in ovarian cancer. *N Engl J Med* 2011;**365**:2484–96.

13. Sandler A, Gray R, Perry MC, Brahmer J, Schiller JH, Dowlati A, Lilenbaum R, Johnson DH. Paclitaxel-carboplatin alone or with bevacizumab for non-small-cell lung cancer. *N Engl J Med* 2006;**355**:2542–50.
14. Yang JC, Haworth L, Sherry RM, Hwu P, Schwartzentruber DJ, Topalian SL, Steinberg SM, Chen HX, Rosenberg SA. A randomized trial of bevacizumab, an anti-vascular endothelial growth factor antibody, for metastatic renal cancer. *N Engl J Med* 2003;**349**:427–34.
15. Kreisl TN, Kim L, Moore K, *et al.* Phase II trial of single-agent bevacizumab followed by bevacizumab plus irinotecan at tumor progression in recurrent glioblastoma. *J Clin Oncol* 2009;**27**:740–5.
16. Bazarbachi A, Abou Merhi R, Gessain A, *et al.* Human T-cell lymphotropic virus type I-infected cells extravasate through the endothelial barrier by a local angiogenesis-like mechanism. *Cancer Res* 2004;**64**:2039–46.
17. El-Sabban ME, Merhi RA, Haidar HA, Arnulf B, Khoury H, Basbous J, Nijmeh J, de Thé H, Hermine O, Bazarbachi A. Human T-cell lymphotropic virus type 1-transformed cells induce angiogenesis and establish functional gap junctions with endothelial cells. *Blood* 2002;**99**:3383–9.
18. Hayashibara T, Yamada Y, Miyanishi T, Mori H, Joh T, Maeda T, Mori N, Maita T, Kamihira S, Tomonaga M. Vascular endothelial growth factor and cellular chemotaxis: a possible autocrine pathway in adult T-cell leukemia cell invasion. *Clin Cancer Res* 2001;**7**:2719–26.
19. Watters KM, Dean J, Gautier V, Hall WW, Sheehy N. Tax 1-independent induction of vascular endothelial growth factor in adult T-cell leukemia caused by human T-cell leukemia virus type 1. *J Virol* 2010;**84**:5222–8.
20. Ito M, Kobayashi K, Nakahata T. NOD/Shi-scid IL2rgnull (NOG) mice more appropriate for humanized mouse models. *Curr Top Microbiol Immunol* 2008;**324**:53–76.
21. Abramoff MD, Magelhaes PJ, Ram SJ. Image Processing with ImageJ. *Biophotonics Int* 2004;**11**:36–42.
22. Imada K, Takaori-Kondo A, Sawada H, Imura A, Kawamata S, Okuma M, Uchiyama T. Serial transplantation of adult T cell leukemia cells into severe combined immunodeficient mice. *Jpn J Cancer Res* 1996;**87**:887–92.
23. Suzuki S, Masaki A, Ishida T, *et al.* Tax is a potential molecular target for immunotherapy of adult T-cell leukemia/lymphoma. *Cancer Sci* 2012;**103**:1764–73.
24. Mori F, Ishida T, Ito A, *et al.* Potent antitumor effects of bevacizumab in a microenvironment-dependent human lymphoma mouse model. *Blood Cancer J* 2012;**2**:e67.
25. Mohammad RM, Wall NR, Dutcher JA, Al-Katib AM. The addition of bryostatin 1 to cyclophosphamide, doxorubicin, vincristine, and prednisone (CHOP) chemotherapy improves response in a CHOP-resistant human diffuse large cell lymphoma xenograft model. *Clin Cancer Res* 2000;**6**:4950–6.
26. Motoi T, Uchiyama T, Uchino H, Ueda R, Araki K. Serum soluble interleukin-2 receptor levels in patients with adult T-cell leukemia and human T-cell leukemia/lymphoma virus type-I seropositive healthy carriers. *Jpn J Cancer Res* 1988;**79**:593–9.
27. Ito A, Ishida T, Utsunomiya A, *et al.* Defucosylated anti-CCR4 monoclonal antibody exerts potent ADCC against primary ATLL cells mediated by autologous human immune cells in NOD/Shi-scid, IL-2R gamma(null) mice *in vivo*. *J Immunol* 2009;**183**:4782–91.
28. Masaki A, Ishida T, Suzuki S, *et al.* Autologous Tax-Specific CTL therapy in a primary adult T cell leukemia/lymphoma cell-bearing NOD/Shi-scid, IL-2Rγnull mouse model. *J Immunol* 2013;**191**:135–44.
29. Wang ES, Teruya-Feldstein J, Wu Y, Zhu Z, Hicklin DJ, Moore MA. Targeting autocrine and paracrine VEGF receptor pathways inhibits human lymphoma xenografts *in vivo*. *Blood* 2004;**104**:2893–902.
30. Koga H, Imada K, Ueda M, Hishizawa M, Uchiyama T. Identification of differentially expressed molecules in adult T-cell leukemia cells proliferating *in vivo*. *Cancer Sci* 2004;**95**:411–7.
31. Yu L, Wu X, Cheng Z, Lee CV, LeCouter J, Campa C, Fuh G, Lowman H, Ferrara N. Interaction between bevacizumab and murine VEGF-A: a reassessment. *Invest Ophthalmol Vis Sci* 2008;**49**:522–7.
32. Ellis LM, Hicklin DJ. VEGF-targeted therapy: mechanisms of anti-tumour activity. *Nat Rev Cancer* 2008;**8**:579–91.
33. Carmeliet P, Jain RK. Principles and mechanisms of vessel normalization for cancer and other angiogenic diseases. *Nat Rev Drug Discov* 2011;**10**:417–27.
34. Jain RK. Normalization of tumor vasculature: an emerging concept in antiangiogenic therapy. *Science* 2005;**307**:58–62.
35. Maemondo M, Inoue A, Kobayashi K, *et al.* Gefitinib or chemotherapy for non-small-cell lung cancer with mutated EGFR. *N Engl J Med* 2010;**362**:2380–8.
36. Bardelli A, Siena S. Molecular mechanisms of resistance to cetuximab and panitumumab in colorectal cancer. *J Clin Oncol* 2010;**28**:1254–61.
37. Lambrechts D, Lenz HJ, de Haas S, Carmeliet P, Scherer SJ. Markers of response for the antiangiogenic agent bevacizumab. *J Clin Oncol* 2013;**31**:1219–30.
38. Ishida T, Joh T, Uike N, *et al.* Defucosylated anti-CCR4 monoclonal antibody (KW-0761) for relapsed adult T-cell leukemia-lymphoma: a multicenter phase II study. *J Clin Oncol* 2012;**30**:837–42.
39. Tanosaki R, Tobinai K. Adult T-cell leukemia-lymphoma: current treatment strategies and novel immunological approaches. *Expert Rev Hematol* 2010;**3**:743–53.
40. Marçais A, Suarez F, Sibon D, Frenzel L, Hermine O, Bazarbachi A. Therapeutic options for adult T-cell leukemia/lymphoma. *Curr Oncol Rep* 2013;**15**:457–64.

Journal of General Virology (2013), **94**, 933–943 DOI 10.1099/vir.0.047167-0

Impact of antiretroviral pressure on selection of primary human immunodeficiency virus type 1 envelope sequences *in vitro*

Shigeyoshi Harada,[1,2] Kazuhisa Yoshimura,[1,2] Aki Yamaguchi,[1] Samatchaya Boonchawalit,[1,2] Keisuke Yusa[3] and Shuzo Matsushita[1]

Correspondence
Kazuhisa Yoshimura
ykazu@nih.go.jp

[1]Center for AIDS Research, Kumamoto University, 2-2-1 Honjo, Chuo-ku, Kumamoto 860-0811, Japan

[2]AIDS Research Center, National Institute of Infectious Diseases, 1-23-1 Toyama, Shinjuku-ku, Tokyo 162-8640, Japan

[3]Division of Biological Chemistry and Biologicals, National Institute of Health Sciences, 1-18-1 Kami-youga, Setagaya-ku, Tokyo 158-8501, Japan

Received 15 August 2012
Accepted 20 December 2012

The initiation of drug therapy results in a reduction in the human immunodeficiency virus type 1 (HIV-1) population, which represents a potential genetic bottleneck. The effect of this drug-induced genetic bottleneck on the population dynamics of the envelope (Env) regions has been addressed in several *in vivo* studies. However, it is difficult to investigate the effect on the *env* gene of the genetic bottleneck induced not only by entry inhibitors but also by non-entry inhibitors, particularly *in vivo*. Therefore, this study used an *in vitro* selection system using unique bulk primary isolates established in the laboratory to observe the effects of the antiretroviral drug-induced bottleneck on the integrase and *env* genes. Env diversity was decreased significantly in one primary isolate [KP-1, harbouring both CXCR4 (X4)- and CCR5 (R5)-tropic variants] when passaged in the presence or absence of raltegravir (RAL) during *in vitro* selection. Furthermore, the RAL-selected KP-1 variant had a completely different Env sequence from that in the passage control (particularly evident in the gp120, V1/V2 and V4-loop regions), and a different number of potential *N*-glycosylation sites. A similar pattern was also observed in other primary isolates when using different classes of drugs. This is the first study to explore the influence of anti-HIV drugs on bottlenecks in bulk primary HIV isolates with highly diverse Env sequences using *in vitro* selection.

INTRODUCTION

Human immunodeficiency virus type 1 (HIV-1) shows a high degree of genetic diversity owing to its high rates of replication and recombination and the high mutation rate of the HIV-1 reverse transcriptase (Nájera *et al.*, 2002). Even in a single infected individual, the virus can best be described as a population of distinct, but closely related, genetic variants or 'quasi-species' (Eigen, 1993; Nijhuis *et al.*, 1998). The quasi-species behaviour of viruses is recognized as a key element in our understanding and modelling of viral evolution and disease control (Vignuzzi *et al.*, 2006).

Combination antiretroviral (ARV) therapy results in a contraction of the viral population, which represents a potential genetic bottleneck (Charpentier *et al.*, 2006; Delwart *et al.*, 1998; Ibáñez *et al.*, 2000; Kitrinos *et al.*, 2005; Nijhuis *et al.*, 1998; Nora *et al.*, 2007; Sheehy *et al.*, 1996; Zhang *et al.*, 1994). Whilst this bottleneck has a direct effect on the region that is being targeted by the drugs (e.g. protease or reverse transcriptase), it also affects other regions of the viral genome. Indeed, the effect of the drug-induced genetic bottleneck on the population dynamics of the envelope (Env) regions has been addressed in several *in vivo* studies (Charpentier *et al.*, 2006; Delwart *et al.*, 1998; Ibáñez *et al.*, 2000; Kitrinos *et al.*, 2005; Nijhuis *et al.*, 1998; Nora *et al.*, 2007; Sheehy *et al.*, 1996; Zhang *et al.*, 1994).

Virus bottleneck evolution of the HIV-1 *env* gene might be important when choosing the optimal drugs to treat a particular patient. Indeed, a CCR5 antagonist (maraviroc, MVC) and a fusion inhibitor (enfuvirtide, T-20) have now

The GenBank/EMBL/DDBJ accession numbers for the *env* sequences of HIV-1 KP-1, KP-2 and KP-4, are AB640872–AB640881, AB641341–AB641351 and AB641335–AB641340, respectively.

Two supplementary figures are available with the online version of this paper.

been approved for use as HIV-1 entry inhibitors. Analysing the dynamics of drug-induced genetic bottlenecks and studying drug-resistant mutation profiles in response to HIV-1-specific ARV drugs are both important if we are to understand fully HIV-1 drug resistance and pathogenesis.

The aim of the present study was to understand better the effect of *in vivo* drug-induced genetic bottlenecks. *In vitro* selection of different primary HIV-1 isolates was performed using the recently approved HIV integrase inhibitor raltegravir (RAL) (Steigbigel *et al.*, 2008). Two R5-, one X4-, one dual- and one mixed R5/X4-tropic isolates were passaged through a RAL-induced genetic bottleneck. We also performed *in vitro* selection of the R5/X4 isolate using lamivudine (3TC), saquinavir (SQV) and MVC, and compared the results with those from the RAL-selected isolate.

RESULTS

Genotypic profiles of the HIV-1 primary isolates

Four genetically heterogeneous HIV-1 primary isolates (KP-1–4) from Japanese drug-naïve patients were used to assess the extent to which RAL affected the selection of bulk primary viruses *in vitro*. A laboratory isolate, strain 89.6, was also used in the study (rather than a molecular clone) to allow escape mutants to be selected from each quasi-species pool and to be generated *de novo*. First, the sequences of the integrase (IN) regions of the four primary isolates were determined. Table 1 shows the detailed evaluation of the R5/X4 mixture subtype B (KP-1), R5-CRF08_BC (KP-2), R5 subtype B (KP-3) and X4-CRF01_AE (KP-4) primary isolates, and the dual-tropic subtype B laboratory virus (89.6). Although some naturally occurring polymorphisms were observed within the IN regions of these isolates compared with the subtype B consensus sequence available from the Los Alamos National Laboratory HIV sequence database, we did not identify any primary resistant mutations to RAL. Three baseline viruses (KP-1, KP-4 and 89.6) were sensitive to RAL, with IC_{50} values ranging from 1.2 to 4 nM, which are comparable with those reported previously (Kobayashi *et al.*, 2008). However, KP-2 and KP-3 showed minor resistance to RAL, with IC_{50} values of 16 and 32 nM, respectively. These two isolates contained amino acid mutations at positions 72, 125 and 201 within the IN region [previously reported as L-870,810 and S-1360 resistance mutations (Hombrouck *et al.*, 2008; Rhee *et al.*, 2008), but not as RAL-resistance mutations]. KP-2 also contained a unique insertion at position 288 (NQDME) at the C-terminal end of the IN region.

In vitro selection of variants of the primary isolates and 89.6 using RAL

To induce RAL-selected HIV-1 variants *in vitro*, PM1/CCR5 cells, a T-cell line expressing high levels of CCR5, were exposed to the four primary isolates and strain 89.6. The viruses were then serially passaged in the presence of RAL. As a control, each isolate was passaged under the same conditions, but without RAL, to allow monitoring of spontaneous changes occurring in the viruses during prolonged PM1/CCR5 cell passage (the passage control). The selected viruses were initially propagated at a RAL concentration equal to each IC_{50} value. The RAL concentrations were then increased from 20 to 85 nM during the course of the selection procedure (Table 1).

Only small shifts in the IC_{50} to RAL were observed in four of the five isolates (KP-1, KP-2, KP-4 and 89.6), with fold changes in IC_{50} values of 3.4, 6.5, 16 and 9.2, respectively. KP-3 did not show resistance to RAL. IC_{50} values in all the passage controls were comparable with those of the baseline viruses (Table 1).

IN region sequences in RAL-selected variants

The full-length *IN* genes were amplified and cloned to determine the genetic basis of selection in the presence or absence of RAL. Ten to 12 clones from each sample were sequenced.

Substitutions within IN were observed at passages 30 (G189R) and 29 (T210I) in two RAL-selected isolates (KP-2 and KP-4, respectively). Neither of these has been reported as IN inhibitor-resistant mutations. No substitutions in the IN regions of KP-3 and 89.6 were found. However, A125T and V180I substitutions were observed in the KP-3 and 89.6 control variants at the last passage. No previously reported mutations were identified in the IN region of KP-1 (an R5/X4 mixture isolate) after 17 passages. However, four amino acids (K7/K111/H216/D278) were selected by RAL from the baseline quasi-species, whereas different amino acids (R7/R111/Q216/N278) were selected in the control-passage variants (Table 1).

Taken together, these findings showed that RAL-induced selection pressure causes adaptation within the IN regions of bulk primary viruses during *in vitro* passage in the target cells, and confirmed that this system can be used to analyse drug-selected variants *in vitro*.

Comparison of *env* gene sequences in RAL-selected and passage-control isolates

A highly diverse gp120 region was observed in the baseline R5/X4 mixture isolate, KP-1; however, the viral diversity of variants passaged in the presence or absence of RAL decreased significantly during *in vitro* selection (overall mean distance after RAL selection of 0.056 at baseline to 0.007 after passage 17; mean overall distance in the passage control of 0.01 after 20 passages, Table 2). Moreover, the RAL-selected and control variants utilized CCR5 to enter the target cell; neither variant used CXCR4 (Table 3).

Interestingly, the low-diversity RAL-selected variant contained a completely different Env sequence from that of the passage-control variant (Fig. 1a). Different regions spanning

Table 1. Susceptibility of HIV-1 isolates to RAL and distinct differences in IN region sequences between RAL-selected and control-passaged viruses

Isolate	Subtype	Tropism	Passage no.	Concn (nM)	RAL-selected variant*		Passage control	
					IN sequence	RAL IC_{50} (nM)	IN sequence	RAL IC_{50} (nM)
KP-1	B	Mix	0	0	*K/R7, K/R111, Q/H216, D/N278*	4	*K/R7, K/R111, Q/H216, D/N278*	4
			8	20	**K**111, **H**216, **D**278	31 (7.8)	**R**7, **R**111, **Q**216, N278	4.5 (1.2)
			17†	20	**K**7, **K**111, **H**216, **D**278	26 (6.5)	**R**7, **R**111, **Q**216, N278	0.4 (0.1)
KP-2	CRF08_BC	R5	0	0	*I201, ins289NQDME*	16	*I201, ins289NQDME*	16
			18	40	G189G/R, *I201, ins289NQDME*	32 (2)	*I201, ins289NQDME*	16 (1)
			30	85	G189R, *I201, ins289NQDME*	55 (3.4)	*I201, ins289NQDME*	25 (1.6)
KP-3	B	R5	0	0	*V72, A125*	32	*V72, A125*	32
			11	25	*V72, A125*	25 (0.78)	*V72, A125*	33 (1)
			22	27.5	*V72, A125*	37 (1.2)	*V72*, A125T	13 (0.41)
KP-4	CRF01_AE	X4	0	0	–	2.1	–	2.1
			8	40	–	33 (16)	R166R/K, D279N	4.4 (2.1)
			29	40	T210I	22 (10)	G163E, R166R/K, D279N/S	4.1 (2)
89.6	B	R5X4	0	0	–	1.2	–	1.2
			8	15	–	34 (28)	–	4.4 (3.7)
			34	20	–	11 (9.2)	V180I	1.2 (1)

*Amino acid changes in each passage variant are shown. Italicized letters represent mutations relative to the consensus subtype BC or B present in the baseline isolates. Bold letters represent amino acids selected out of the quasi-species cloud. The fold increase in RAL IC_{50} values is shown in parentheses for *in vitro*-selected variants compared with those in the baseline isolates.
†The RAL variant selected after 17 passages was compared with the control selected after 20 passages.